
Wave-current interactions: numerical model implementation and assessment in the Mediterranean Sea

Technical Notes

January 2024
Issue TN0298

*OPA – Ocean
Predictions and
Applications*

*By Aimie Moulin
Fondazione CMCC
Centro Euro-
Mediterraneo sui
Cambiamenti Climatici
aimie.moulin@cmcc.it*

*Emanuela Clementi
Fondazione CMCC
Centro Euro-
Mediterraneo sui
Cambiamenti Climatici
emanuela.clementi@
cmcc.it*

*The research leading to
these results has received
funding from the IMMERSE
project.*

SUMMARY

This report describes the wave-current interaction processes recently implemented in the Ocean General Circulation Model NEMO (Nucleus for European Modelling of the Ocean) version 4.2 in the framework of the IMMERSE H2020 Project (<https://cordis.europa.eu/project/id/821926>) and assesses the impacts of those new developments, especially the effect of the wave-induced mixing in the Mediterranean sea dynamics. A set of sensitivity experiments are performed using the hydrodynamic model NEMO v4.2 coupled with the spectral wave model WaveWatchIII (WW3) v6.07 through the OASIS library. The configuration is based on the operational Copernicus Marine Service Mediterranean forecasting physical system (MedFS). Both models are implemented at $1/24^\circ$ resolution and are forced by European Centre for Medium-Range Weather Forecasts (ECMWF) $1/10^\circ$ horizontal resolution atmospheric fields. The models are one-way coupled therefore the wave model is sending fields every hour to the hydrodynamic model. Two-year numerical experiments are carried out in both uncoupled and coupled mode. In order to validate the system, numerical results are compared with in-situ and observational data. This study is focused on the coupling on upper-ocean properties (such as temperature, salinity and surface currents) and mixed layer depth, at mesoscale. The sensitivity of the ocean dynamic to wave-current interactions is also evaluated during a specific extreme event.

Keywords wave-current, NEMO 4.2, Mediterranean Sea



1- INTRODUCTION

Ocean and atmosphere dynamics are governed by complex processes at their interface, including momentum, energy, and heat fluxes. The sea state is intimately involved in these exchange processes (Ardhuin et al., 2005). An accurate representation of ocean surface waves is recognized as essential for ocean forecasting systems and operational oceanography (Onink et al., 2019; Breivik et al., 2015; Shimura et al., 2017). The increased availability of computational resources allowed for coupled ocean-wave models and taking wave effects into account for ocean and trajectory models has been an effort during recent years (Hasselmann, 1991; Rascle and Ardhuin, 2009; Law Chune and Aouf, 2018).

Waves impact the ocean dynamics in three major ways: the momentum transfer, the turbulent energy injection and the generation of mass transport (Cavaleri et al., 2012).

Waves regulate the sea surface roughness and modulate the amount of momentum transferred from the atmosphere to the ocean surface layer (Janssen, 2008). The physics behind the momentum flux transfer depend on the dynamics of the wave field and more especially on the wind–wave growth, the nonlinear wave–wave interactions and the wave dissipation. Those processes cannot be parameterized in a hydrodynamic model and can only be adequately represented by a wave model.

Waves also induce mixing in the upper ocean layer via two processes, the wave breaking and the surface wave average flow generating Langmuir cells. The wave breaking injects turbulent kinetic energy into a layer with a depth of the order of the significant wave height, whereas transport of turbulence to a deeper part of the ocean could occur due to the generation of Langmuir cells (Leibovich, 1980). Couvelard et al (2020) and Belcher et al. (2012) have demonstrated that Langmuir turbulence is important over wide areas of the global ocean to deepen the Mixed Layer Depth.



Assessment of wave-current effects on the circulation in the Med-MFC system

The irregular waves induce an additional mass transport called Stokes drift (Stokes, 1847) in the direction of wave propagation. It is a consequence of the fact that fluid parcels spend more time in the forward-moving region under the crest (with larger velocities) than the backward-moving region under the trough (van den Bremer and Breivik, 2017). Near the surface, this drift can become substantial and decreases exponentially with depth. The Stokes drift interacts with the Coriolis force and the relative vorticity field, which gives rise to the physical interaction processes respectively called Stokes-Coriolis (Hasselmann, 1971) and vortex-force (Craig and Leibovich, 1976). Lewis and Belcher (2004) showed that Stokes Coriolis force deflects the surface current by about 10 to 20 degrees farther to the right (NH) compared to steady Ekman balance (Polton et al., 2005).

All these complicated feedback mechanisms can be modelled by coupling hydrodynamic and wave numerical models, which have usually been developed separately since a few years ago. Different levels of complexity exist to account for the wave's impact on the wind stress, the Stokes drift and the wave-enhanced mixing in hydrodynamical models.

In the context of IMMENSE WP-5 (Task 5.2), the air-sea coupling through surface waves improved in the NEMO model so that NEMO version 4.2 includes a larger number of wave fields from an external wave model, which can be used to activate wave-current interaction processes. Currently, 13 wave fields could be transferred to NEMO v4.2 instead of 6 for NEMO v4.0. and the new implemented wave-current interaction process are coded following Couvelard et al. (2020).

In case of ocean-wave coupled systems, currents are separated into a quasi-Eulerian mean current and the Stokes drift. The Stokes drift is calculated with the Breivik et al. (2016) parameterization using the surface Stokes drift and the associated Stokes transport from a wave model. NEMO v4.2 can take into account the Stokes-Coriolis, the vortex force, and the Bernoulli head pressure terms for the calculation of



CMCC Technical Notes

the Eulerian mean currents. An important point to make here is that the Eulerian mean current can be affected by wave mixing. The most important changes in NEMO v4.2 concern the Turbulent Kinetic Energy closure scheme. The surface boundary condition for TKE can now be calculated with a Neumann boundary condition accounting for the energy flux Φ_{oc} from waves to the ocean. The shear production term now takes into account the Stokes drift. The Langmuir turbulence parameterization is improved including the Stokes Drift contribution using Craik-Leibovich velocity scale. Changes in the ECMWF bulk formulae are included to take into account the effect of waves in the wind stress calculation. More details of the implementation of the wave-current interaction can be found in the NEMO v4.2 reference manual and summarised in the following Section 2.

An accurate representation of wave-current dynamical processes is of particular relevance to operational forecasting systems, thus these modeling advancements are tested into the Mediterranean forecasting system which operational within the Copernicus Marine Service (called MedFs). The Mediterranean operational system is composed by a basic 2-way coupled hydrodynamic-wave model, where the hydrodynamics are supplied by NEMO while the wave component is provided by WaveWatch-III (WW3). The coupling between the hydrodynamic model and the wave model consists in exchanging the following fields: NEMO sends to WW3 the air-sea temperature difference and the surface currents, while WW3 sends to NEMO the neutral drag coefficient used to evaluate the surface wind stress (Clementi et al., 2017a). In such a configuration, the hydrodynamic changes are negligible at large space and time scales, becoming more evident when considering the coupling impacts during storm events (Clementi et al., 2017a). A stronger coupling between waves and currents by improving the representation of their interactions as well as accounting for a wave-enhanced mixing into the Copernicus Marine Mediterranean operational system could be of fundamental importance to improve the representation of the basin dynamics.



Assessment of wave-current effects on the circulation in the Med-MFC system

In this study, NEMO v4.2 model including upgraded ocean–wave interaction processes is coupled to WW3 v6.07 through OASIS and implemented in the Mediterranean Sea. The aim of this study is to assess the impact of the new developments on wave-current interactions, especially the effect of the wave-induced mixing and the Langmuir turbulence in the Mediterranean Sea dynamics in order to improve in a future release of the Mediterranean Forecasting System.

The first part of the report presents a short resume of the wave-current interaction processes that are introduced in NEMO v4.2 and tested for this report. The second part describes the modelling system and its set-up in the Mediterranean Sea. The third part describes the set of numerical experiments that are performed. The fourth part is dedicated to the models (NEMO and WW3) validation. It presents an inter-comparison between uncoupled experiments with NEMO v3.6 and NEMO v4.2 including a validation of the Mediterranean Sea configuration using NEMO v4.2. The fifth part focuses on the effect of waves on the Mediterranean dynamics during a 2-year period and for a specific extreme event. Finally, a summary and conclusions are provided.

2- WAVE-CURRENT IMPLEMENTATION IN NEMO VERSION 4.2 COUPLED MODE

NEMO v4.2 is extended to incorporate additional physical processes related to ocean surface waves. In this section, we detail the processes that are included in the hydrodynamic-wave coupled simulations carried out in the Mediterranean Sea (see Section 4). They can be divided in three main categories: modified wind stress, inclusion of the Stokes drift and associated forces, and enhanced vertical mixing.

In our coupled simulations, the neutral drag coefficient from the wave model can be used to evaluate the wind stress as detailed in [Clementi et al. \(2017a\)](#). Using the bulk formulae from the MedFS system and starting from the neutral coefficient provided by the wave model, the drag coefficient is computed according to the stable/unstable conditions of the air-sea interface following [Large and Yeager \(2004\)](#), instead of being parameterized following the [Hellerman and Rosenstein \(1983\)](#) formulation.



CMCC Technical Notes

The second modification considers the Stokes drift. A more accurate evaluation of the Stokes drift vertical profile and related processes is included in NEMO v4.2 in order to improve the representation of the ocean circulation. A velocity profile based on the Phillips spectrum which is considered to be a reasonable estimate of the part of the spectrum mostly contributing to the Stokes drift velocity near the surface (Breivik et al., 2016) is used (Eq 1a and 1b).

$$U_s(z) = |U_s|_{z=0} \left[e^{2k_p z} - \beta \sqrt{-2k_p \pi z} \operatorname{erfc}(\sqrt{-2k_p z}) \right] \quad (\text{Eq. 1a})$$

$$k_p = |U_s|_{z=0} \left(1 - 2 \frac{\beta}{3} \right) 2 |T_s| \quad (\text{Eq. 1b})$$

where erfc is the complementary error function, $\beta = 1$ and k_p is the peak wavenumber. The surface Stokes drift ($|U_s|_{z=0}$) and the Stokes transport (T_s) are provided directly by the wave model.

The Stokes drift enters the wave-averaged momentum equation, as well as the tracer advection equations. In NEMO v4.2, the momentum equation includes the Stokes-Coriolis force (already in NEMO v4.0), the vortex-force, and the Bernoulli head J pressure term (Eq. 2).

$$\frac{du}{dt} + u \nabla \cdot u + f \times u + \frac{1}{\rho} \nabla P - \frac{d}{dz} \left(K_z \frac{du}{dz} \right) = -f \times U_s + U_s \times \nabla \times u - \nabla J \quad (\text{Eq. 2})$$

In a rotating ocean, waves exert a wave-induced stress on the mean ocean circulation which results in a force named Stokes-Coriolis equal to $U_s \times f$ where f is the Coriolis parameter. This additional force may have an impact on the Ekman turning of the surface current. The vortex-force term arises from the interaction of the mean flow vorticity with the Stokes drift. It results in a force equal to $U_s \times \zeta$, where ζ is the mean flow vorticity. An adjustment in the mean pressure arises to accommodate for the presence of waves. The mean pressure is corrected by adding a depth-uniform wave-induced kinematic pressure term named Bernoulli head J term. The Bernoulli head J



Assessment of wave-current effects on the circulation in the Med-MFC system

term is provided to NEMO from the external wave model, where it is defined as :

$$J = g \frac{\iint k}{\sinh} (2kd) S(k, \theta) dk d\theta \quad (\text{Eq. 3})$$

with d the water depth, S the wave spectrum depending on the wave number (k) and wave direction (θ).

Main changes related to the wave-current interactions included in NEMO v4.2 concerns the impact of surface waves on the vertical mixing via the modification of the surface boundary conditions for the Turbulent Kinetic Energy closure scheme, the inclusion of the Stokes drift contribution to the shear production term in the TKE turbulent closure schemes and the parameterization of the Langmuir turbulence.

Waves give rise to extra terms in the turbulent kinetic energy (TKE) prognostic (Couvelard et al., 2020). The first term corresponds to a modification of the shear production term to take into account the contribution of the Stokes drift shear. In addition, waves affect the surface boundary condition for the turbulent kinetic energy, the mixing length scale and the dissipative length scale of the TKE closure scheme. The mixing length scale surface value is estimated from the surface roughness length (z_0) which is, in coupled mode, directly estimated from the significant wave height (H_s) provided by the external wave model as $z_0 = 1.6H_s$. The injection of turbulent kinetic energy at the surface can be given by the dissipation of the wave field, usually dominated by wave breaking. In coupled mode, the wave to ocean energy flux term (Φ) from an external wave model can be provided and then converted into an ocean turbulence source. Due to the definition of the computational grid, the TKE flux is not applied at the free surface but at the centre of the topmost grid cell ($z = z_1$). To be more accurate, in coupled mode, a Neumann boundary condition amounting to interpreting the half-grid cell at the top as a constant flux layer (consistent with the surface layer Monin–Obukhov theory) is applied as in Eq. 4 (Couvelard et al., 2020).



CMCC Technical Notes

$$\left(\frac{K_m}{e_{3t}} \partial_k e \right)_{z=z_1} = \frac{\Phi}{\rho_o} \quad (\text{Eq. 4})$$

being K_m the vertical eddy viscosity, e_{3t} the NEMO vertical scale factor, k the layer, and ρ_o the ocean density.

Some improvements are introduced in the Langmuir turbulence parameterization if wave coupled mode is activated. The extra source term in the TKE equation, P_{LC} related to the Langmuir circulation (LC) is assumed to be:

$$P_{LC}(z) = \frac{\omega_{LC}^3(z)}{H_{LC}} \quad (\text{Eq. 5})$$

where $\omega_{LC}(z)$ is the vertical velocity profile of LC, and H_{LC} is the LC depth.

ω_{LC} is defined as:

$$w_{LC} = \begin{cases} c_{LC} \|u_s^{LC}\| \sin(-\pi z/H_{LC}) & \text{if } -z \leq H_{LC} \\ 0 & \text{otherwise} \end{cases} \quad (\text{Eq. 6})$$

where c_{LC} is an adimensional parameter for the Langmuir circulation

In the absence of information about the wave field, LC is assumed to be proportional to the surface Stokes drift empirically estimated by $U_s^{LC} = 0.377 |\tau|^{1/2}$, where $|\tau|$ is the surface wind stress module. Whereas in the case of online coupling with the external wave model, LC is proportional to the $U_s^{LC} = \max(U_{s0} \cdot e_\tau, 0)$ where e_τ is the unit vector in the wind stress direction and U_{s0} is the surface Stokes drift provided by the external wave model.

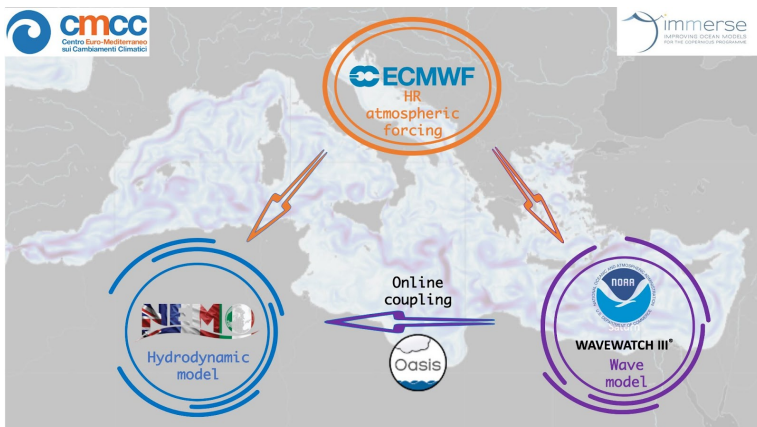
The adimensional parameter c_{LC} is set through the NEMO namelist parameter and should range between 0.15 and 0.54 (Axell, 2002). $c_{LC} = 0.15$ is chosen by Axell (2002) as a good compromise to fit Large Eddy-Simulations (LES) data whereas in Couvelard et al. (2020) c_{LC} is set to 0.3 based on a series of single-column simulations.



3- MEDITERRANEAN SEA CONFIGURATION

The Mediterranean hydrodynamic-wave coupled system (Figure 1) used to assess the impact of waves in the basin is based on NEMO version 4.2 and WaveWatch-III (WW3) spectral wave model (version 6.07). The OASIS Model Coupling Toolkit (OASIS3-MCT) version 4 (Craig et al., 2017) is used for data exchange and synchronisation between the two models. Details of each model configuration are provided in the following.

Figure 1. One way coupled system



3.1- CIRCULATION MODEL COMPONENT (NEMO)

The Mediterranean Sea configuration is based on the operational Copernicus Marine Service Mediterranean analysis and forecasting physical system (MedFS).

The oceanic equations of motion of MedFS are solved by NEMO which is implemented in the Mediterranean Sea at $1/24^\circ \times 1/24^\circ$ (ca. 3.5 km) horizontal resolution and 141 unevenly spaced vertical levels (Clementi et al., 2017b) with a time step of 120 sec. The model covers the whole Mediterranean Sea and also extends into the Atlantic in order to better resolve the exchanges with the Atlantic Ocean at the Strait of Gibraltar (Figure 2). The topography is created starting from the GEBCO 30 arc-second grid (http://www.gebco.net/data_and_products/gridded_bathymetry_data_gebco_30_second_grid/), filtered (using a Shapiro filter) and manually modified in



CMCC Technical Notes

critical areas such as: islands along the Eastern Adriatic coasts, Gibraltar and Messina straits, Atlantic box edge.

The NEMO code solves the primitive equations using the time-splitting technique that is the external gravity waves are explicitly resolved with non-linear free surface formulation and time-varying vertical z-star coordinates. The advection scheme for active tracers, temperature and salinity, is a mixed up-stream/MUSCL (Monotonic Upwind Scheme for Conservation Laws; Van Leer, 1979), originally implemented by Estubier and Lévy (2000) and modified by Oddo et al. (2009). The vertical diffusion and viscosity terms are a function of the Richardson number, as parameterized by Pacanowsky and Philander (1981).

The model interactively computes air-surface fluxes of momentum, mass, and heat. The bulk formulae implemented are described in Pettenuzzo et al. (2010) and are currently used in the Mediterranean operational system (Tonani et al., 2015). A detailed description of other specific features of the model implementation can be found in Oddo et al. (2009, 2014).

The vertical background viscosity and diffusivity values are set to $1.2e-6$ [m^2/s] and $1.0e-7$ [m^2/s] respectively, while the horizontal bilaplacian eddy diffusivity and viscosity are set respectively equal to $-1.2e8$ [m^4/s] and $-2.e8$ [m^4/s]. A quadratic bottom drag coefficient with a logarithmic formulation is used according to Maraldi et al. (2013) and the model uses vertical partial cells to fit the bottom depth shape.

The model is forced by momentum, water and heat fluxes interactively computed by bulk formulae using the 6-hours temporal resolution and the $1/10^\circ$ horizontal-resolution analysis fields from the European Centre for Medium-Range Weather Forecasts (ECMWF) and the model predicted surface temperatures (details of the air-sea physics are in Tonani et al., 2008). The water balance is computed as Evaporation minus Precipitation and Runoff. The evaporation is derived from the latent heat flux, precipitation is provided by ECMWF as daily averages, while the runoff of the 39 rivers



Assessment of wave-current effects on the circulation in the Med-MFC system

implemented is provided by monthly mean climatological data. The incoming water from Dardanelles Strait is introduced here as a river runoff.

The model is nested in the Atlantic within the Copernicus Marine Global analysis and forecasting system daily data set at 1/12° horizontal resolution and 50 vertical levels (Copernicus Marine product GLOBAL_ANALYSIS_FORECAST_PHY_001_024). In particular, a Flather boundary condition is imposed for the barotropic velocities at the Atlantic (South, West, East) as well as a flow relaxation scheme is used for baroclinic velocities and tracers.

The Turbulent Kinetic Energy closure scheme is used in all the simulations in order to assess the impact of the new development including the wave-induced mixing. Based on [Delrosso \(2020\)](#), the uncoupled experiment uses the classical setup for the TKE i.e. there is no wave-induced mixing parameterization except for the Langmuir cells parameterization [\(Axell, 2002\)](#). It estimates the surface Stokes drift (U_s) from the 10m wind as $U_s = 0.016 \cdot U_{10m}$.

The major modelling implementation of the configuration testes are in Table 1.

Table 1. List of the major modelling implementation characteristics in the IMMENSE T5.2 experiments.

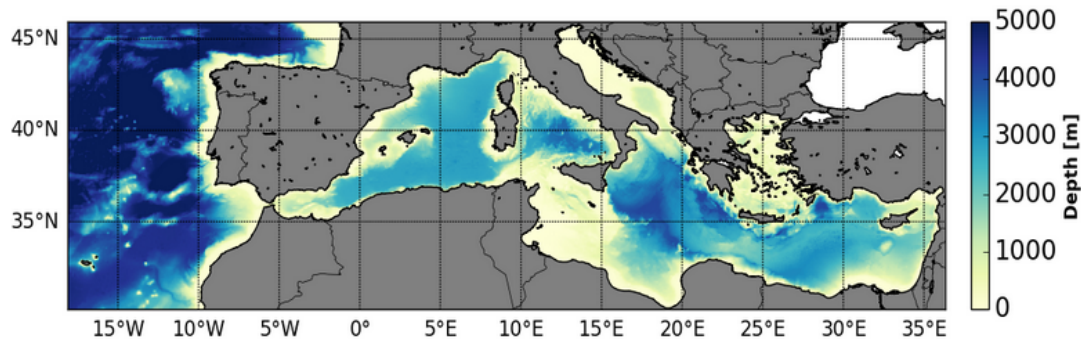
	IMMERSE T5.2 config.
Model version	NEMO v4.2, WW3 v6.07
Coupler	OASIS3 MCT v4.0
Tides	no
Vertical mixing scheme	TKE
NEMO Lateral Open Boundary	<u>Atlantic</u> : Tracers & baroclinic vel = Flow Relaxation; Barotropic vel = Flather. <u>Dardanelles</u> : Closed (parameterized as a river)



3.2- WAVE MODEL COMPONENT (WW3)

The Wave dynamic is solved by a Mediterranean implementation of the WaveWatch-III (WW3) code version 6.07 (WW3 Manual, 2019). WaveWatch covers the same domain (Figure 2) and follows the same horizontal discretization of the circulation model ($1/24^\circ \times 1/24^\circ$) with a global time step of 360 sec.

Figure 2. Model domain and bathymetry (in m)



The wave model uses 24 directional bins (15° directional resolution) and 30 frequency bins (ranging between 0.0573 Hz and 1.1 Hz) to represent the wave spectral distribution.

WW3 is forced by the same $1/10^\circ$ horizontal resolution ECMWF atmospheric forcing as the hydrodynamic model. WW3 model solves the wave action balance equation that describes the evolution, in slowly varying depth domain and currents, of a 2D ocean wave spectrum where an individual spectral component satisfies locally the linear wave theory. In the present application, WW3 is implemented using third-order Ultimate Quickest propagation scheme (UQ, Tolman, 2002b) with the Garden Sprinkler correction (Tolman, 2002a).

Wind input and dissipation terms are based on the wind-wave interaction semi-empirical source terms (ST4) (Ardhuin et al., 2010). The non-linear wave-wave



Assessment of wave-current effects on the circulation in the Med-MFC system

interaction is modelled using the Discrete Interaction Approximation (DIA, Hasselmann et al., 1985). Wave-bottom interactions, depth-induced breaking (Battjes and Janssen, 1978), and the reflection off the shoreline are included.

For this configuration, a close domain is considered, thus swell is not entering through the Atlantic boundaries.

3.3- MODEL COUPLING (OASIS LIBRARY)

For this study, the models are one-way online coupled using the OASIS3-MCT version 4 library. In the coupled implementation, the wave model is sending fields every hour to the hydrodynamic model (one-way). When all the coupled processes are activated, the following fields are provided from WW3 to NEMO: the significant wave height (H_s), the mean wave period (T0M1), the surface Stokes-drift components (USS, VSS) and the associated transport (TUS, TVS), the neutral drag coefficient (C_{dn}), the Bernoulli head J term (Bhd) and the wave to ocean energy flux term (ϕ_{ioc}).

It is worth noting that all the wave fields (including the zonal and meridional Stokes Drift and transport components) are provided on the tracer T-grid.

4- NUMERICAL EXPERIMENTS DESCRIPTION

Two uncoupled experiments using NEMO v3.6 (CTRL_TKE_v36) and NEMO v4.2 (TKE_v42) are run to assess the differences between the two model versions. TKE_v42 experiment represents the control run for the coupled experiments. A list of the main characteristic of the experiments is provided in Table 2.

The two uncoupled experiments are run for 3 years (2018–2020) considering 2018 as a spin-up. Coupled experiments are initialised from 1st January 2019 using the restart from the TKE_v42 uncoupled experiment.

The analyses are provided for the 2-year period from 1st January 2019 to the 31st December 2020.

**Table 2: List of the numerical experiments**

EXP	NEMO version	Key	WAVE COUPLING				
			Neutral Cd from wave	Stokes drift	VF+SC+BHD	Mixing	Langmuir coeff
CTRL_TKE_v36	3.6	key_vvl	NO	NO	NO	NO	0.15
TKE_v42	4.2	key qco	NO	NO	NO	NO	0.15
TKE_CO_CD	4.2	key qco	YES	NO	NO	NO	0.15
TKE_CO_MIX_LC03	4.2	key qco	NO	YES	YES	YES	0.3
TKE_CO_FORCE_MIX_LC015	4.2	key qco	YES	YES	YES	YES	0.15
TKE_CO_FORCE_MIX_LC03	4.2	key qco	YES	YES	YES	YES	0.3

5 - MODEL VALIDATION

5.1 - INTERCOMPARISON BETWEEN NEMO V3.6 AND V4.2 UNCOUPLED EXPERIMENTS

This section considers only the two uncoupled experiments: CTRL_TKE_v36 and TKE_v42. The first subsection consists in the validation of the CTRL_TKE_v36 and TKE_v4.2 experiments by comparing numerical model results with respect to available *in-situ* and satellite data derived from Copernicus Marine observations over the Mediterranean basin. In a second subsection, results are inter-compared by means of time series of daily mean fields averaged in the whole basin at different depths (for 3D fields) as well as yearly and seasonally averaged maps at the surface.

5.1.1- VALIDATION OF CTRL_TKE_V36 AND TKE_V42 EXPERIMENTS

The estimated accuracy numbers (EANs), as defined in the Copernicus Marine Service framework, are used in order to validate the experiments. They are composed



Assessment of wave-current effects on the circulation in the Med-MFC system

of the mean and the root-mean-square namely Bias and RMSD of the difference between the model outputs and *in-situ* or satellite observational data.

The EANs are evaluated for CTRL_TKE_V36 and TKE_V42 experiments over the 2-year period. Results are computed over 9 vertical layers and for 16 subregions (Figure 3):

(1) Alboran Sea, (2) South West Med 1 (western part), (3) North West Med, (4) South West Med 2 (eastern part), (5) Tyrrhenian Sea 2 (southern part), (6) Tyrrhenian Sea (northern part), (7) Ionian Sea 1 (western part), (8) Ionian Sea 2 (south-eastern part), (9) Ionian Sea 2 (north-eastern part), (10) Adriatic Sea 2 (southern part), (11) Adriatic Sea 1 (northern part), (12) Levantine Sea 1 (western part), (13) Aegean Sea, (14) Levantine Sea 2 (central-northern part), (15) Levantine Sea 3 (central southern part), (16) Levantine Sea 4 (eastern part).

Figure 3. The Mediterranean Sea sub-regions subdivision for validation metrics

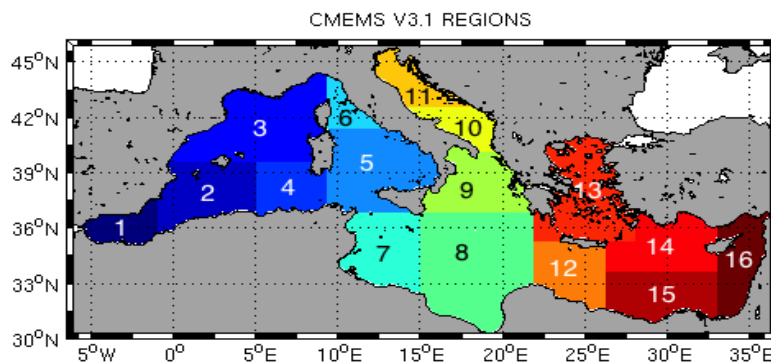


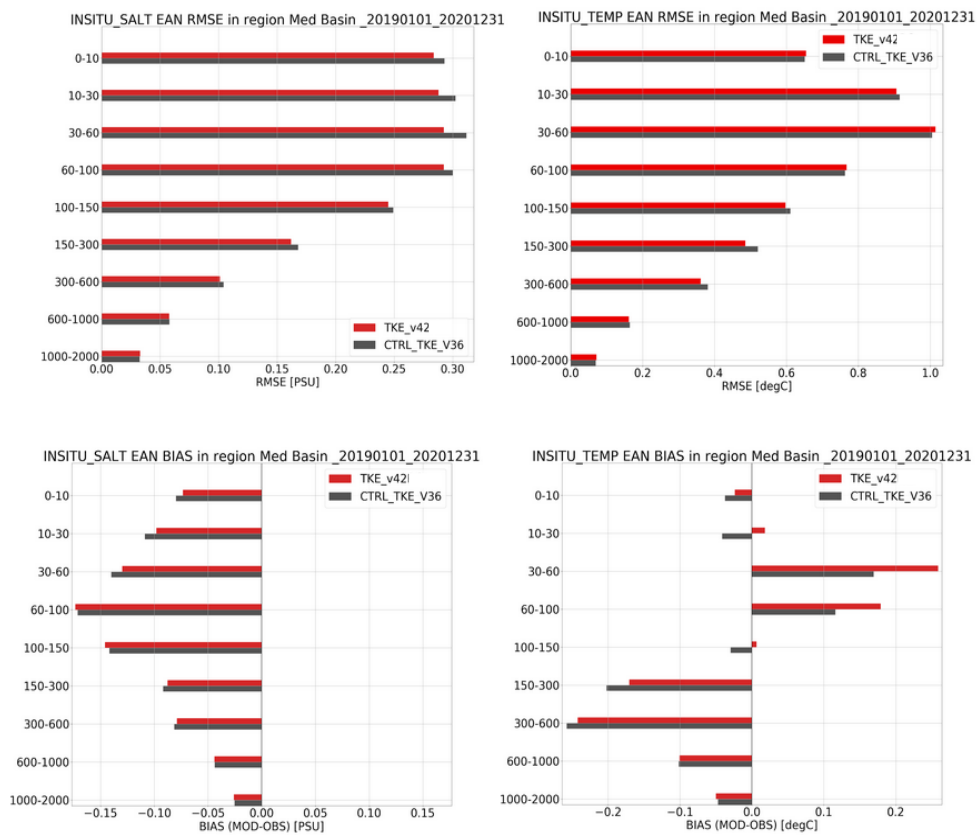
Figure 4 shows models' daily mean salinity (left) and temperature (right) compared to *in-situ* observations (ARGO floats from Copernicus Marine product *in-situ_MED_NRT_OBSERVATIONS_013_035*) in terms of RMSD and BIAS (model



CMCC Technical Notes

minus observations), averaged in the period 2019-2020 and in the whole Mediterranean Sea along 9 vertical layers.

Figure 4. Salinity [PSU] (left) and temperature [°C] (right) RMSD (top) and BIAS (bottom) evaluated comparing the daily mean model outputs of the TKE_v42 (red) and the CTRL_TKE_v36 (dark grey) experiments with respect to in-situ observations in the period 2019-2020 and averaged along 9 vertical layers.



The average error of the 2 experiments presents a slight improvement in both salinity and temperature for the TKE_v42 experiment in comparison to the CTRL_TKE_v36. The new version of the code presents a smaller salinity RMSD especially at the surface and in the sub-surface layers (until 100m depth) with respect to NEMO v3.6. The BIAS in salinity is negative in all the layers for both experiments



Assessment of wave-current effects on the circulation in the Med-MFC system

and is slightly reduced for TKE_v42 except for the 60-150m layer. The temperature RMSD is similar for both experiments in the first 100m whereas it is slightly improved between 100 and 600m for the latest NEMO version. The BIAS in temperature is globally decreased for all the layers with NEMO v4.2 except between 30 and 100m depth.

Figure 5. Sea surface temperature [°C] RMSD evaluated comparing the daily mean model outputs of the TKE_v42 (red) and the CTRL_TKE_v36 (dark grey) experiments with respect to satellite observations in the period 2019-2020 in the whole basin (Med), 16 sub-regions as in Figure 3 and Atlantic box (Atl)

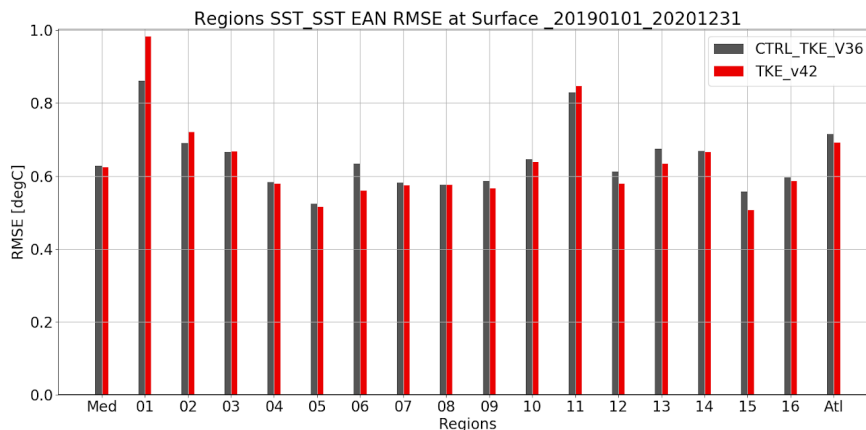
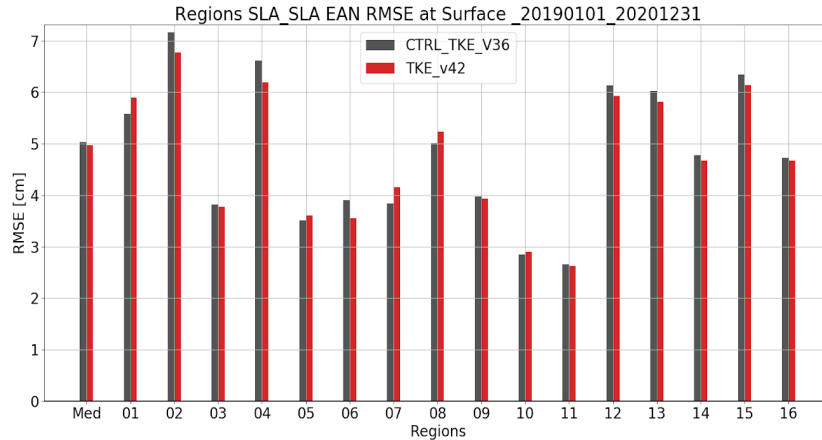


Figure 5 shows the models' daily mean sea surface temperature (SST) compared to satellite L4 gridded observations (product SST_MED_SST_L4_NRT_OBSERVATIONS_010_004) in terms of RMSD averaged in the period 2019-2020 in the whole Mediterranean region and in the 16 subregions and the Atlantic subregion (Figure 3). The average errors of the two experiments is similar when considering the whole Mediterranean Sea, while several differences can be observed in sub-regional domains. We can observe a small reduction of the RMSD for the TKE_v42 in almost all the areas except the Alboran Sea (region 1), the South West Med 1 (region 2) and the Northern Adriatic Sea (region 11). Major differences in the RMSD of the daily mean SST are observed in smaller areas, thus characterised by a lower number of observations.



Figure 6. Sea level anomaly [cm] RMSD evaluated comparing the daily mean model outputs of the TKE_v42 (red) and the CTRL_TKE_v36 (dark grey) experiments with respect to satellite observations in the period 2019-2020 in the whole basin (Med) and 16 sub-regions as in Figure 3.



Basin and sub-basin averages of the sea level anomaly (SLA) RMSD (Figure 6) evaluated comparing model outputs to along-track altimeter data (product SEALEVEL_EUR_PHY_L3_NRT_OBSERVATIONS_008_059) are similar for both experiments with a slight improvement in most of the subregions for the NEMO v4.2 experiment.

In conclusion, results from the NEMO v4.2 simulation show to improve the representation of the Mediterranean Sea, providing a solution which is slightly closer to the observations (both *in-situ* and satellite data).

5.1.2 INTER-COMPARISON OF CTRL_TKE_V36 AND TKE_V42 EXPERIMENTS

In this subsection, we are inter-comparing the results of the experiments from both versions of NEMO in order to better identify the differences between the 2 implementations.



Assessment of wave-current effects on the circulation in the Med-MFC system

Figure 7 shows the temperature daily mean time series evaluated as basin average, at the surface (top panel) and for the whole water column (3rd panel). The differences between the two NEMO version experiments for the surface and the whole water column are respectively emphasised in the 2nd and bottom panels. In both experiments, atmospheric fluxes give rise to a seasonal pattern at the surface and in the sub-surface layer (not shown) with the highest temperature in summer. The temperature of the NEMO v4.2 experiment is cooler at the surface in summer whereas the temperature is warmer in winter months with respect to the NEMO v3.6 run. Nevertheless, differences between both experiments are negligible (less than 0.05°C at the surface). Considering the differences in the whole basin, a slight increase of the mean temperature is visible for the more recent NEMO version.

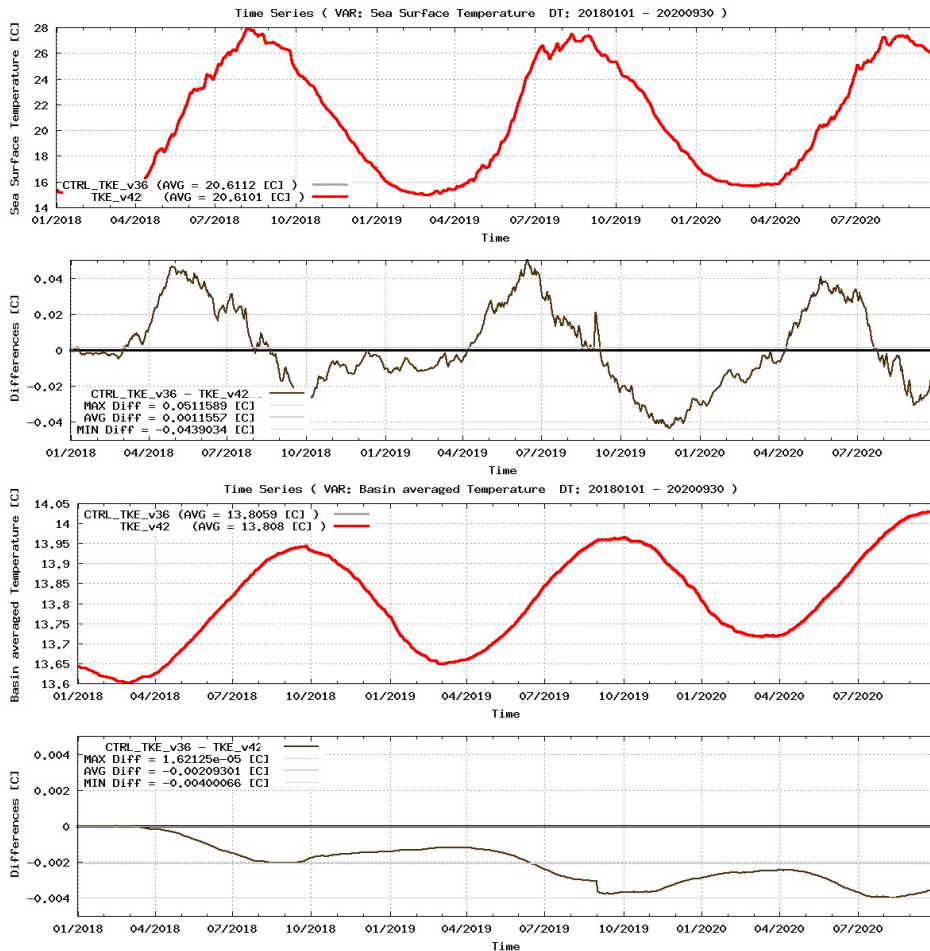
As for the temperature, Figure 8 shows the salinity daily mean time series evaluated as basin averages, at the surface (top panel) and for the whole water column (3rd panel) and the respective differences between NEMO v3.6 and NEMO v4.2 (2nd and bottom panels). As expected, in both versions, experiments are reproducing the seasonal variability of the surface salinity with a larger salinity in autumn and lower in spring. NEMO v4.2 simulation shows, at the surface, a slightly higher salinity in winter whereas it is lower in summer with respect to NEMO v3.6 simulation. The basin averaged salinity shows a slight increased trend in the daily mean for both NEMO v3.6 and NEMO v4.2. The basin averaged salinity for the NEMO v42 experiment is slightly larger than the one from NEMO v3.6 experiment, in the whole water column nevertheless this difference is negligible (less than 0.001 PSU) and as for temperature we notice a slight increase of salinity in NEMO v4.2.



20

CMCC Technical Notes

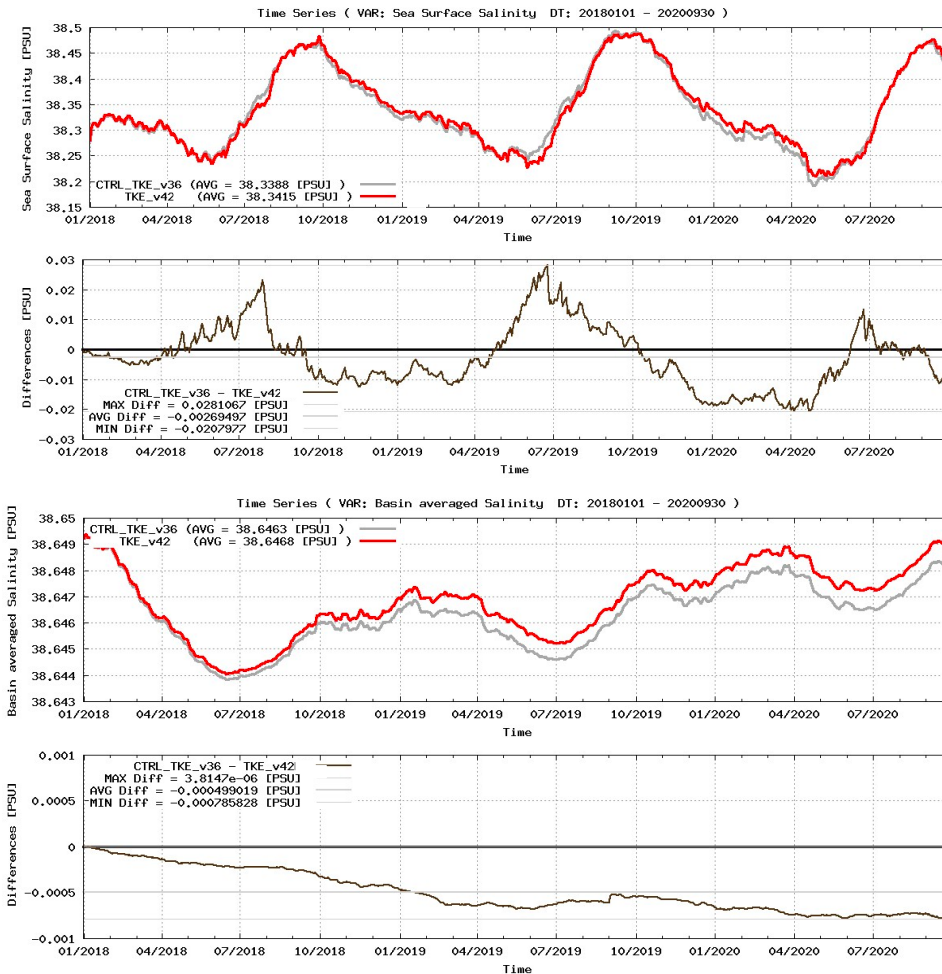
Figure 7. Time series of daily mean model temperature [°C] averaged in the whole Mediterranean Sea, at the surface (top panel), and integrated in the whole column (3rd panel) for the control run NEMO v3.6 (grey line) and NEMO v4.2 (red line). The temperature mean values for each layer is reported in the legend for the 2 experiments. Temperature difference between NEMO v3.6 and NEMO v4.2: mean, minimum and maximum difference values at the surface (2nd panel) and integrated in the whole column (bottom panel).





Assessment of wave-current effects on the circulation in the Med-MFC system

Figure 8. Time series of salinity [PSU] averaged in the whole Mediterranean Sea, at the surface (top) and integrated in the whole column (3rd panel) for the control run NEMO v3.6 (grey) and NEMO v4.2 (red). The salinity mean values for each layer are reported in the legend for the 2 experiments. Salinity difference between NEMO v3.6 and NEMO v4.2: mean, minimum and maximum difference values at the surface (2nd panel) and integrated in the whole column (bottom panel).



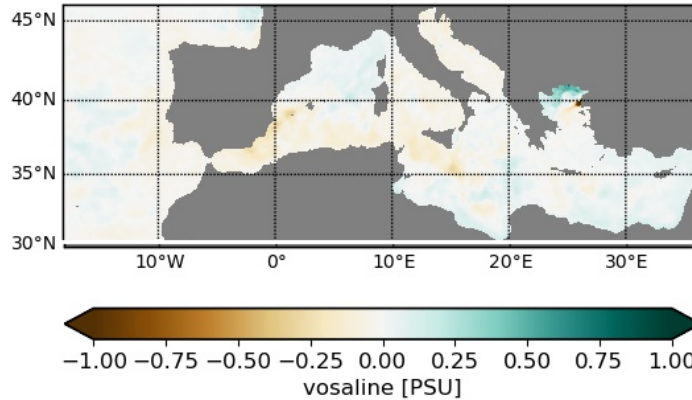
Small differences in the basin averaged temperature and salinity is observed between the simulations but are negligible and could be attributed to changes in the code between NEMO v4.2 and NEMO v3.6.



CMCC Technical Notes

Figure 9 Surface (8 m depth) maps of time mean (2019-2020) differences between NEMO v3.6 and NEMO v4.2 salinity (top panel) and temperature (bottom panel).

DIFF -(CTRL_TKE_v36 - TKE_v42 MEAN vosaline [PSU] - DEPTH: 8[m] - DT: 20190101_20201231



DIFF -(CTRL_TKE_v36 - TKE_v42 MEAN votemper [degC] - DEPTH: 8[m] - DT: 20190101_20201231

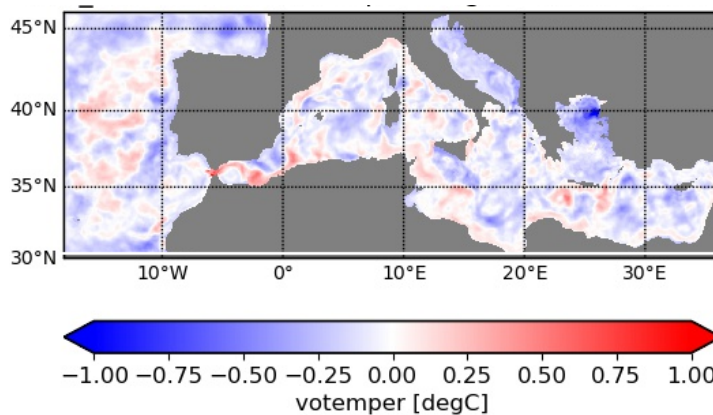


Figure 9 is presenting the salinity difference (top panel) and temperature difference (bottom panel) between the 2 experiments (NEMO v3.6 minus NEMO v4.2) averaged in the 2-year period (2019-2020) at 8m depth. Major differences are noticed in the area of the Dardanelles Strait that shows a clear warming and higher salinity close to the strait with respect to the control run. The difference could be attributed to the improved river runoff modelling implementation in the recent version of NEMO (since the Dardanelles Strait flux in the Mediterranean Sea is here represented as a river inflow).

Assessment of wave-current effects on the circulation in the Med-MFC system

In order to assess the model ability to reproduce the Mixed Layer Depth (MLD), monthly averaged 2D maps of MLD are compared to a climatological dataset available from literature (Houpert et al., 2015) providing monthly gridded climatology produced using MBT, XBT, Profiling floats, Gliders, and ship-based CTD data from different databases and carried out in the Mediterranean Sea between 1969 and 2013. Figure 10 shows the 2D maps of climatological MLD from literature (left), monthly averaged MLD from NEMO v3.6 (middle) and monthly averaged MLD from NEMO v4.2 (right) for February (top panels), August (middle panels) and December (bottom panels) in the period 2019-2020.

It can be noticed that during February 2019-2020 (Figure 10, top line), the deepening of the MLD in the Gulf of Lyon and in the South Adriatic areas are well represented by the model, which present for these years a deeper MLD in the Aegean Sea than the one shown in the climatological fields.

During August 2019-2020 (Figure 10, second line) the modelled MLD is in general very similar to the climatological one, showing a low MLD. In December 2019 (Figure 10, bottom line) the deepening of the MLD is well represented by both simulations.

In general, it can be noticed that both numerical simulations are able to represent the spatial and seasonal distribution of the MLD and the main differences can be due to the low resolution of the climatological dataset that moreover do not cover the whole domain of the Mediterranean Sea as well as on the different period of evaluation, being the Mediterranean Sea characterised by areas of deep-water formation whose intensity can significantly vary in time.

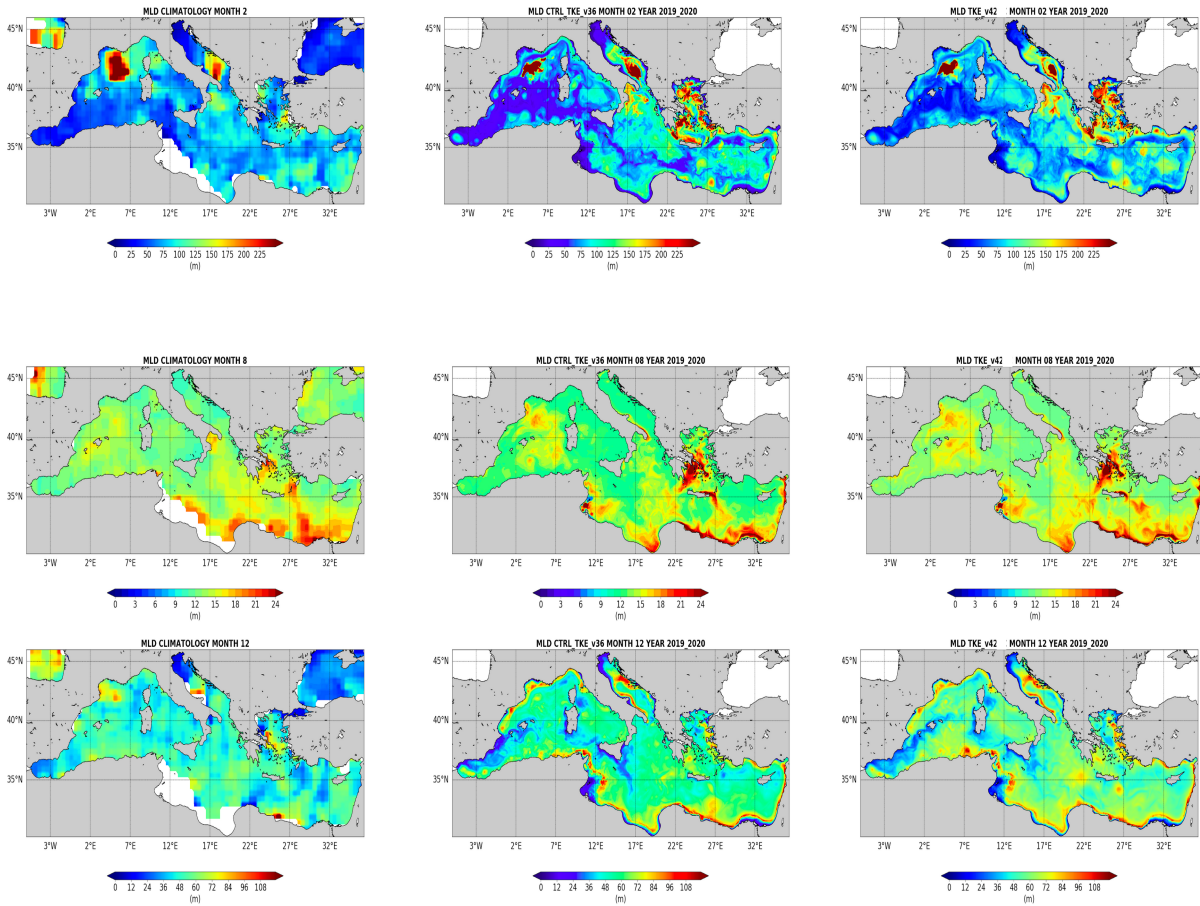
Differences in the MLD daily mean over the whole Mediterranean domain between the 2 experiments (Figure 11) are almost null in summer and up to a few metres in winter (when the water column is highly mixed). The time averaged difference is around 0.5m.





CMCC Technical Notes

Figure 10. February (top), August (middle), December (bottom) MLD 2D maps of the climatological data from literature (left). February, August, December 2019-2020 monthly averaged MLD from NEMO v3.6 (middle) and NEMO v4.2 (right).



The 2019-2020 MLD time mean map (Figure 12) shows that highest differences are observed in the Gulf of Lion, which is an area of strong convection and deep MLD (hundreds of metres) in winter.



Assessment of wave-current effects on the circulation in the Med-MFC system

Figure 11. Time series of the MLD [m] averaged in the whole Mediterranean Sea (top panel). MLD difference between NEMO v3.6 and NEMO v4.2: mean, minimum and maximum difference values (bottom panel).

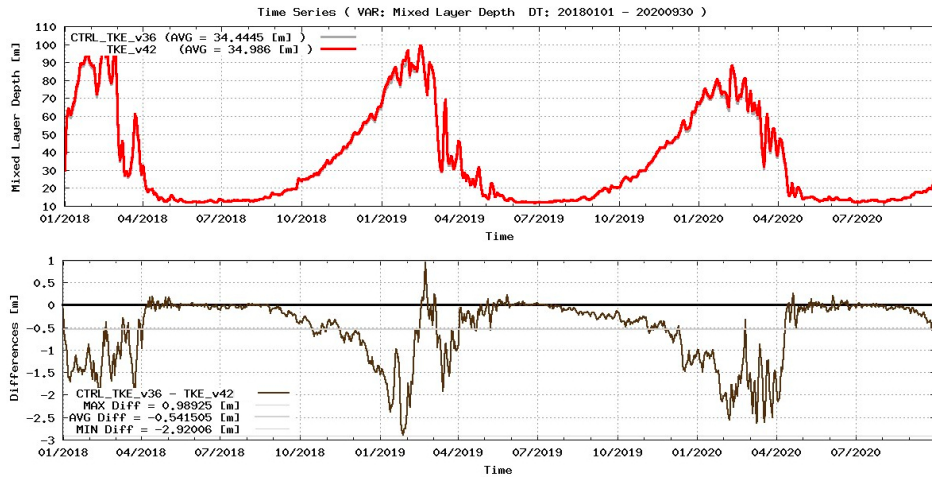
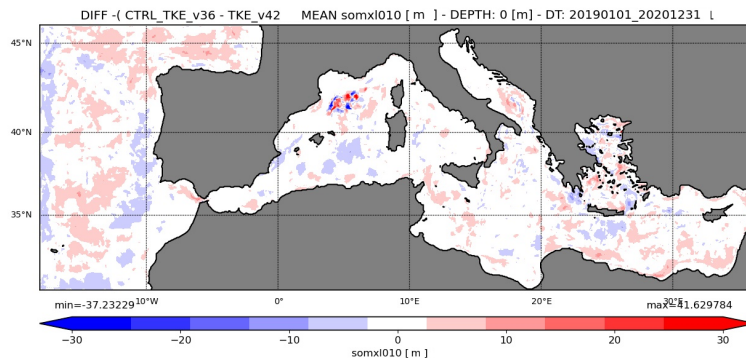


Figure 12. Map of MLD time mean (2019-2020) differences [m] between NEMO v3.6 and NEMO v4.2.



The daily mean Sea Surface Height (SSH) timeseries inter-comparison among the two experiments is shown in Figure 13. After a few days, simulations start to diverge to reach an almost constant SSH difference with a SSH of about 4cm larger in NEMO v4.2. The increased sea level is evident in the whole Mediterranean basin with only a few areas presenting a decreased sea level as seen in the 2019-2020 SSH time mean



CMCC Technical Notes

map (Figure 14). This almost constant difference may be attributed to the modification of the vertical scale factor implementation between NEMO v3.6 and NEMO v4.2.

Figure 13. Time series of the sea surface height (SSH) [m] averaged in the whole Mediterranean Sea (top panel). SSH difference between NEMO v3.6 and NEMO v4.2: mean, minimum and maximum difference values (bottom panel).

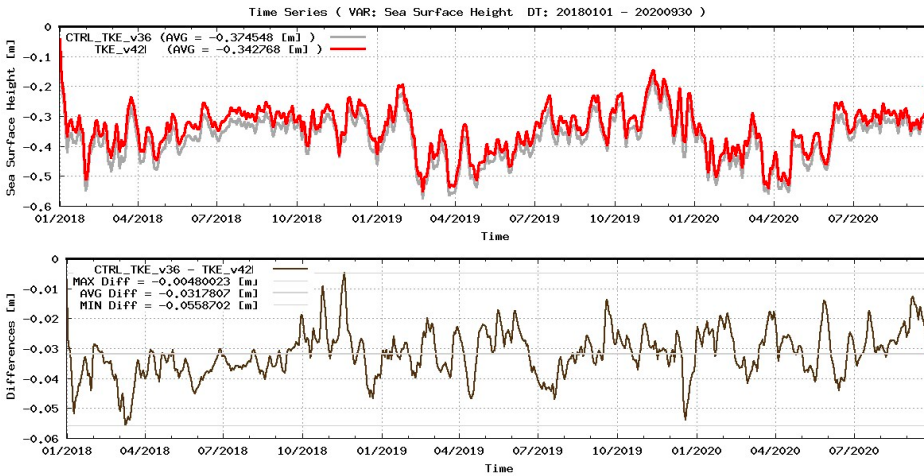
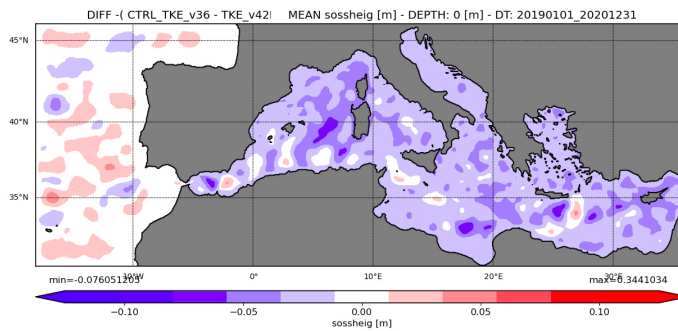


Figure 14. Map of Sea Surface height (SSH) time mean (2019-2020) differences [m] between NEMO v3.6 and NEMO v4.2.



The last inter-comparison is focused on the Total Kinetic Energy integrated in the whole Mediterranean domain. The surface kinetic energy is of the same order of



Assessment of wave-current effects on the circulation in the Med-MFC system

magnitude for both simulations, with daily mean differences less than 3% between NEMO v3.6 and NEMO v4.2 (Figure 15). Considering the basin average (Figure 16), the TKE_v42 simulation is always more energetic than the CTRL_TKE_v36 with a larger daily energy up to 10%.

Figure 15. Time series of the Kinetic Energy (KE) [m²/s²] averaged in the whole Mediterranean Sea (top panel). KE difference between NEMO v3.6 and NEMO v4.2: mean, minimum and maximum difference values (bottom panel).

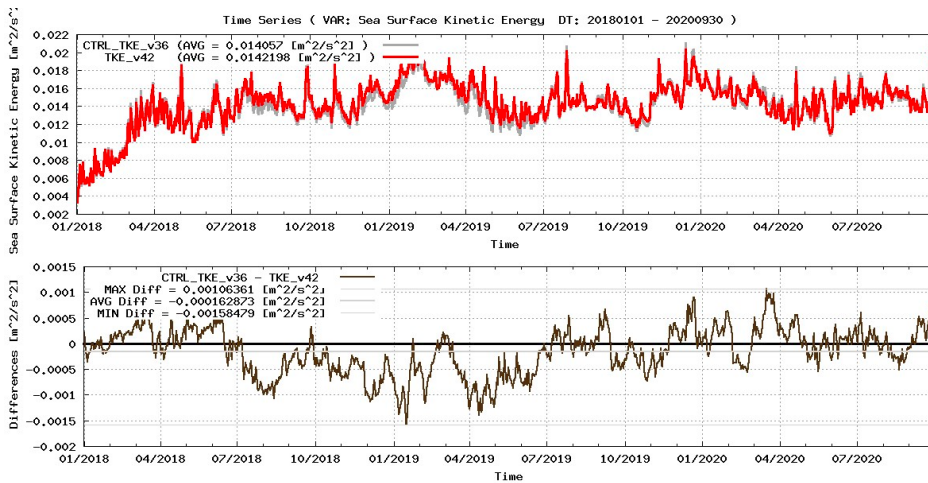
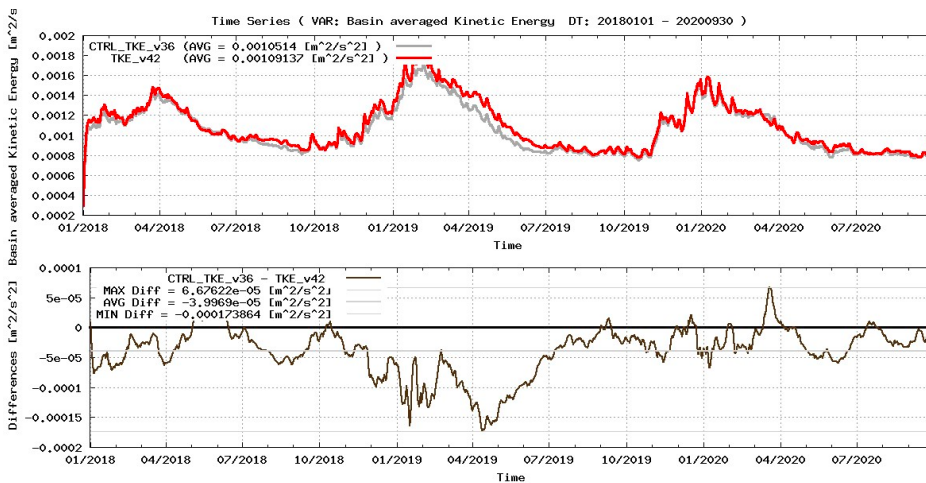


Figure 16. Time series of the Kinetic Energy (KE) [m²/s²] averaged in the whole Mediterranean Sea (top panel). KE difference between NEMO v3.6 and NEMO v4.2: mean, minimum and maximum difference values (bottom panel).



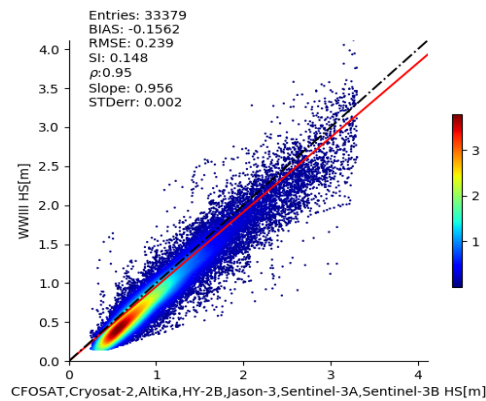


5.2- WW3

In this section, we provide an assessment of the wave model which is used in the coupled experiments.

The WW3 significant wave heights output for the 2-year period 2019-2020 are compared with satellite observations (Figure 17). The model results fit the altimeter data with a correlation coefficient of 0.956. The BIAS between the model and the observation is of -0.16m *i.e.* the model sub-estimate the significant wave height, especially for the lower values.

Figure 17. Scatter plots of significant wave height (HS) [m] comparison between satellite data and numerical results for 2019 to 2020. Dot colours refer to the data probability density; black dashed line represents the best-fit (1:1) line; solid red line shows the satellite-model data fit.



6- ASSESSMENT OF THE WAVE-CURRENT INTERACTIONS

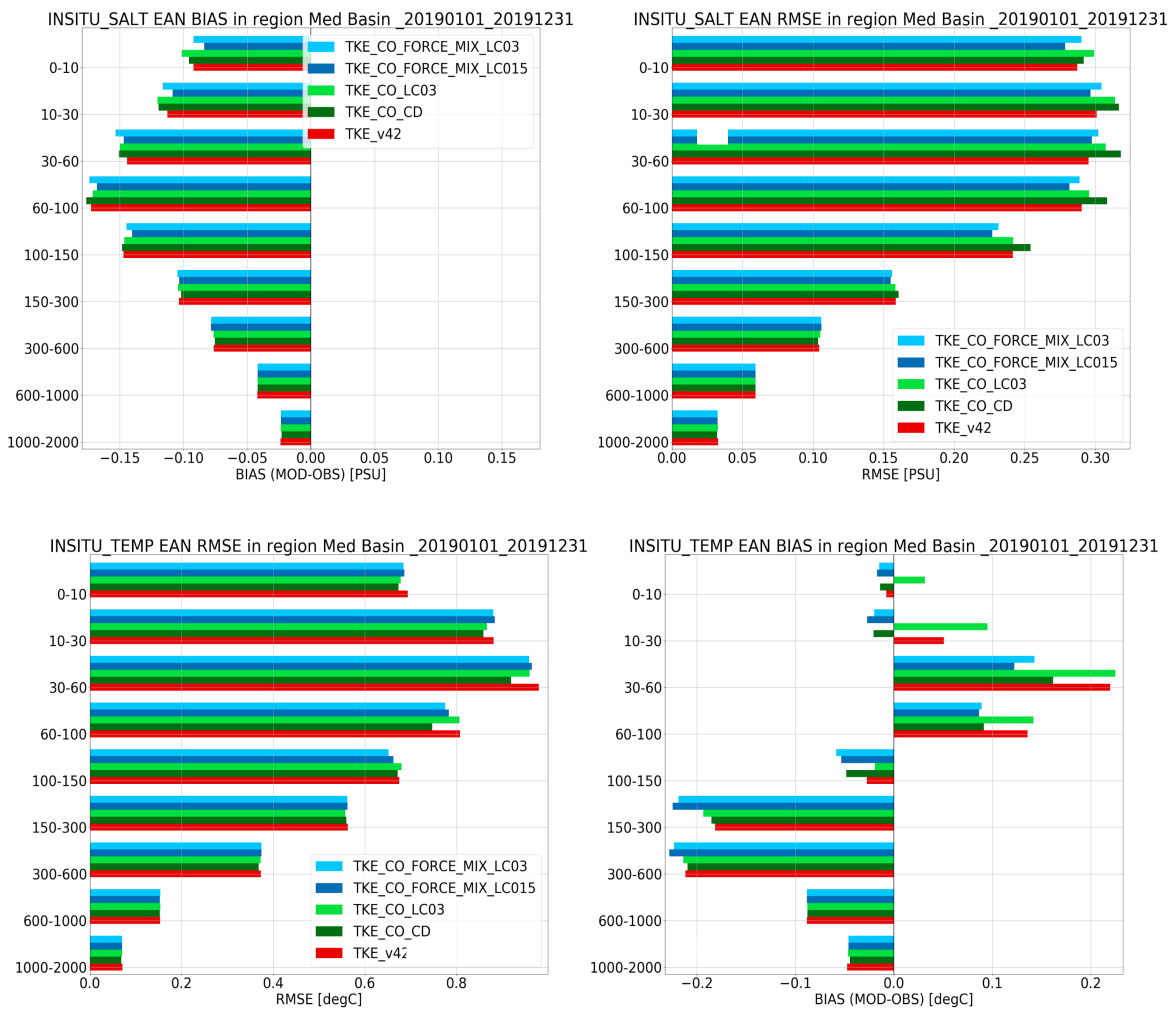
This section provides an assessment of the NEMO-WW3 coupled experiments and is divided into two subsections. The first one focuses on the comparison of model outputs with observational data (*in-situ* and satellite). The second part consists in an assessment of the wave-current interactions in the Mediterranean Sea.



Assessment of wave-current effects on the circulation in the Med-MFC system

6.1 - COMPARISON OF MODEL OUTPUTS WITH IN-SITU AND SATELLITE DATA

Figure 18. Salinity [PSU] (left) and temperature [°C] (right) RMSD (top) and BIAS (bottom) evaluated comparing the daily mean model outputs with respect to in-situ observations in the 2019 year for the whole Mediterranean Sea and averaged along 9 vertical layers. Different colours represent different experiments, as listed in the legend and described in Table 2.

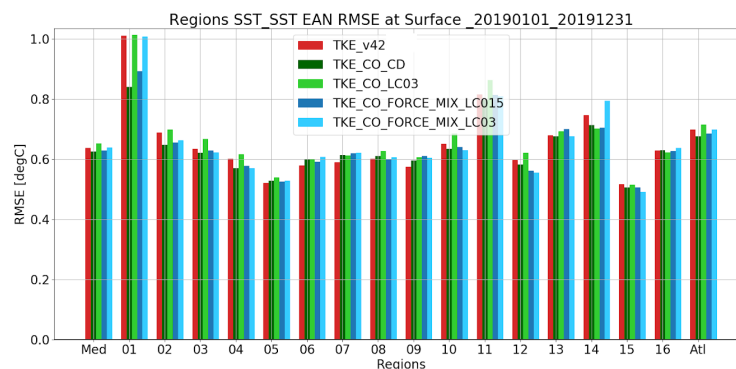


CMCC Technical Notes

An analysis based on Estimated Accuracy Numbers (as detailed in subsection 4.a) is provided in order to assess the impact of wave-current interactions on the Mediterranean Sea temperature and salinity by comparing model results with respect to *in-situ* observations (ARGO floats from Copernicus Marine product *in-situ_MED_NRT_OBSERVATIONS_013_035*). RMSD and BIAS are calculated for the uncoupled TKE_42 and for each coupled simulation described in section 3 (and listed in Table 2), for the year 2019 (Figure 18). The experiment coupled only by means of the surface drag coefficient from the wave model (TKE_CO_CD) shows the largest improvement in the temperature RMSD and BIAS especially in the first 150m, whereas it leads to a larger error in the salinity.

All the coupled experiments slightly decrease the temperature RMSD with respect to the uncoupled experiment, whereas only the TKE_CO_FORCE_MIX_LC015 experiment, including the whole set of coupling processes with a Langmuir parameter (c_{LC}) decreased to 0.15, reduces the salinity RMSD and BIAS in the first 150m. The choice of the adimensional Langmuir parameter is of great importance for the Mediterranean Sea dynamics. As observed, simulations using $c_{LC}=0.3$ present a larger salinity error and bias, whereas the experiment using $c_{LC}=0.15$ improves both temperature and salinity skill.

Figure 19. Sea surface temperature [°C] RMSD evaluated comparing the daily mean model outputs of the uncoupled TKE_v42 (red) and the coupled experiments (as listed in the legend and described in Table 2) with respect to satellite observations for the year 2019 in the whole basin (Med), 16 sub-regions (as in Figure 3) and Atlantic box (Atl).



Assessment of wave-current effects on the circulation in the Med-MFC system

The models' daily mean sea surface temperature (SST) is compared to satellite L4 gridded observations (Copernicus Marine product SST_MED_SST_L4_NRT_OBSERVATIONS_010_004) in terms of RMSD averaged for 2019 in the Medsea region and in the 17 subregions including the Atlantic subregion (Figure 19). Considering the whole basin, all the experiments are characterised by a similar mean error of about 0.6°C. Several differences can be detected considering sub-regional errors, where the experiment coupled by the surface drag coefficient (TKE_CO_CD) and the one including all the coupling processes with a decreased Langmuir coefficient (TKE_CO_FORCE_MIX_LC015) provide the greatest improvement in terms of SST skill. The Alboran Sea is characterised by the largest error reduction (more than 0.1°C) with respect to the uncoupled experiment.

Considering the computational effort, only the uncoupled experiment TKE_v42 and the coupled experiment TKE_CO_FORCE_MIX_LC015, that showed the major improvements for both temperature and salinity in comparison with *in-situ* and satellite data, are extended for an additional year (2020). Temperature and salinity EANs analysis results for the 2-year period are plotted in Figure 20. As for the 2019 period, the basin averaged salinity RMSD and BIAS are slightly decreased over the whole water column for the fully coupled experiment. When considering the temperature, we can observe a slight reduction of the error, while the BIAS clearly decreases between 30 and 150m whereas the layer from 10 to 30m presents some deterioration. As expected, bottom layers do not seem to be affected by the wave-coupling. Even though the basin averaged temperature and salinity model errors in comparison to *in-situ* data, are decreasing for the fully coupled experiment TKE_CO_FORCE_MIX_LC015, results strongly depend on the Medsea sub-regions (figures not shown).

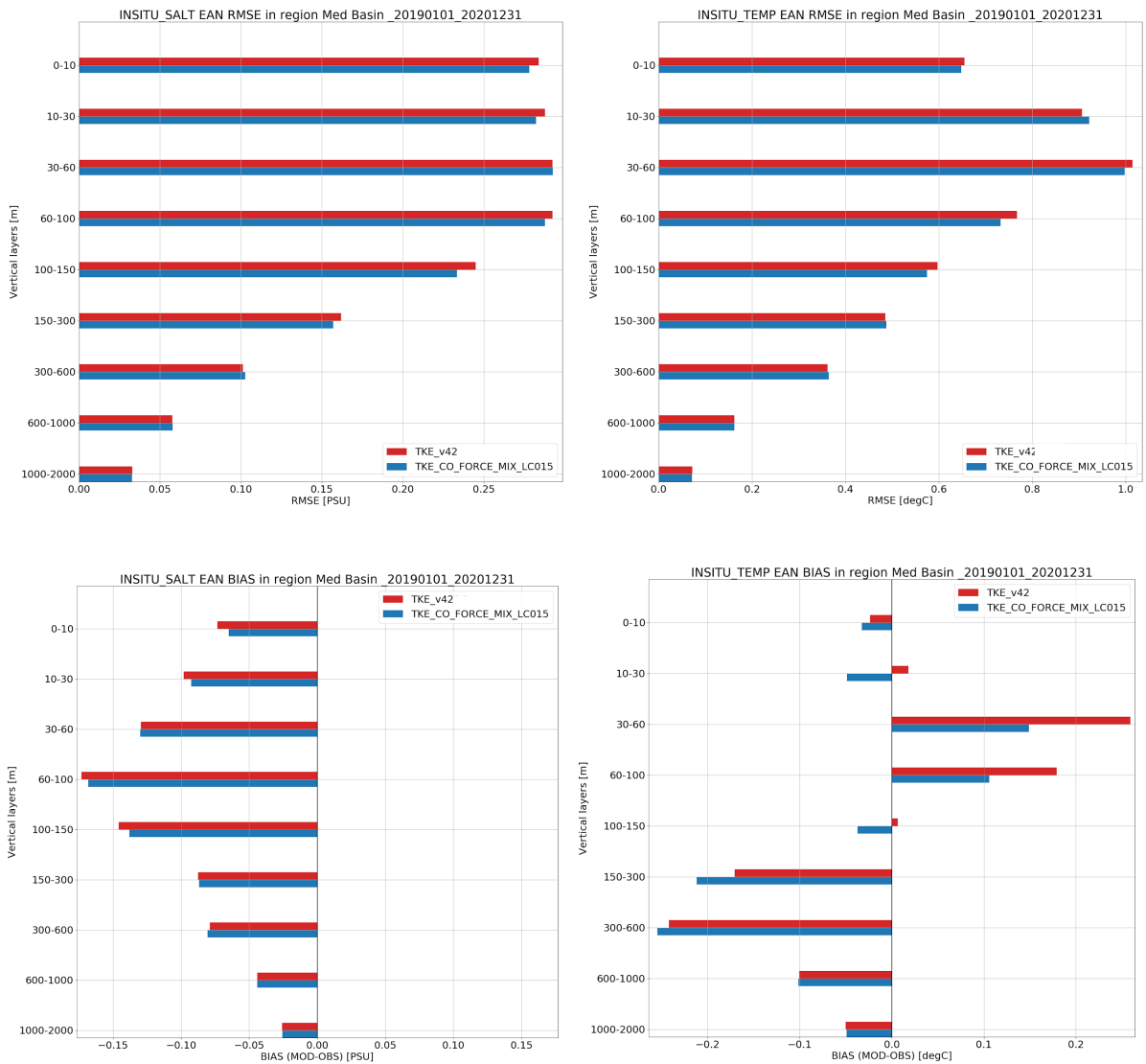


31



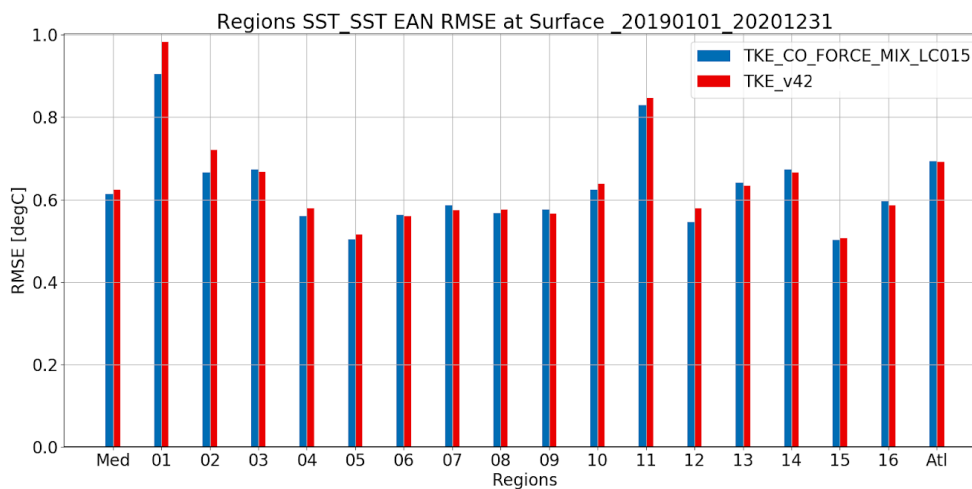
CMCC Technical Notes

Figure 20. Salinity [PSU] (left) and temperature [°C] (right) RMSD (top) and BIAS (bottom) evaluated comparing the daily mean model outputs with respect to in-situ observations for the 2-year period 2019-2020 for the whole Mediterranean Sea and averaged along 9 vertical layers. The red and blue bars are respectively for the uncoupled experiment (TKE_v42) and the fully coupled experiment (TKE_CO_FORCE_MIX_LC015).



EANs analysis of the SST for the 2019-2020 period (Figure 21), shows a slight improvement of the averaged basin SST and especially in the Western area of the basin when coupling with waves is included.

Figure 21. Sea surface temperature [°C] RMSD evaluated comparing the daily mean model outputs of the uncoupled TKE_v42 (red) and the coupled TKE_CO_FORCE_MIX_LC015 (blue) with respect to satellite observations for the 2-year period 2019-2020 in the whole basin (Med), 16 sub-regions (Figure 3) and Atlantic box (Atl).



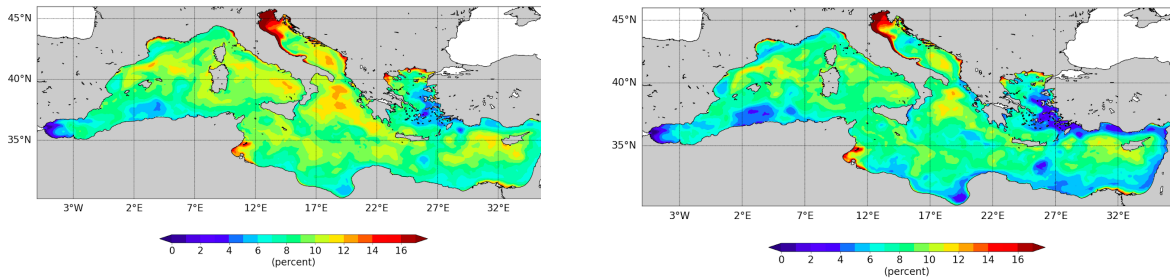
In order to analyse the spatial differences between model results and satellite SST data, maps of differences between the observations and the simulations (in percentage) averaged in the 2-year period are shown in Figure 22. Both uncoupled and coupled simulations are, on average, cooler than the observations over the whole Mediterranean. TKE_CO_FORCE_MIX_LC015 simulation shows a lower BIAS than the uncoupled experiment, especially in the Aegean Sea, Levantine Sea and the western part of the Mediterranean Sea.

Areas of larger differences are mainly located in the Northern Adriatic Sea, which is an area affected by a large observational uncertainty.



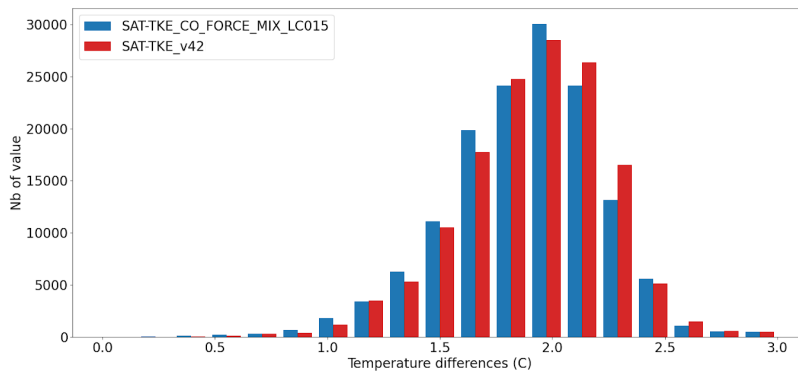
CMCC Technical Notes

Figure 22. Maps of SST time mean (2019-2020) differences [%] between model outputs and satellite observations for the uncoupled experiment (TKE_v42) (left) and the fully coupled run (TKE_CO_CD_LC015) (right).



In order to evidence the lower SST BIAS of the coupled experiment, the BIAS distribution is plotted in Figure 23. It clearly shows that a large part of the basin is characterised by a 2°C difference between model and satellite SST and that the coupled experiment presents a globally smaller difference with respect to the uncoupled one.

Figure 23. Distribution of the time mean (2019-2020) sea surface temperature BIAS [°C] for the coupled TKE_CO_FORCE_MIX_LC015 (blue) and the uncoupled TKE_v42 (red) experiments.



Assessment of wave-current effects on the circulation in the Med-MFC system

In conclusion, the fully coupled experiment i.e. with the surface drag coefficient provided by the wave model, the Stokes-drift calculated with the Breivik et al. (2016) formulation, the Vortex Force, Stokes Coriolis, Bernoulli Head pressure terms, the wave-induced mixing and the Langmuir cells (with $c_{LC}=0.15$) implemented by modifying the TKE closure scheme as in Couvelard et al. (2020) shows a statistical improvement in temperature and salinity. The choice of the adimensional Langmuir parameter value (c_{LC}) seems to play an important role in those simulations, as the results are only improved for the simulation with the $c_{LC}=0.15$. This coefficient may be adjusted in the future depending on the study area.

The analysis of the time evolution of monthly mean RMSD (Figure 24) and BIAS (Figure 25) for salinity and temperature shows similar order of magnitude for the uncoupled and coupled experiments. The coupled experiment shows a slight improvement in the temperature RMSD and BIAS (3rd and 4th panels in Figures 24 and 25) especially from September 2019 to March 2020. The temperature RMSD at the surface layers presents a seasonal pattern with higher error in summer and autumn than winter and spring, as expected since during periods of intense stratification the correct representation of the thermocline becomes more challenging. The temperature RMSD in the 0-60m is almost the same in both experiments, whereas salinity (1st panel in Figure 25) is slightly better for the coupled experiment during autumn and winter. For the 60-150m layers (2nd and 4th panels), an improvement of the skill for both salinity and temperature is observed after 7 months. The salinity BIAS (1st and 2nd panel in Figure 26) is always negative (thus both implementations are underestimating the observed salinity) and is lower for the coupled experiment especially from August 2019 to March 2020.

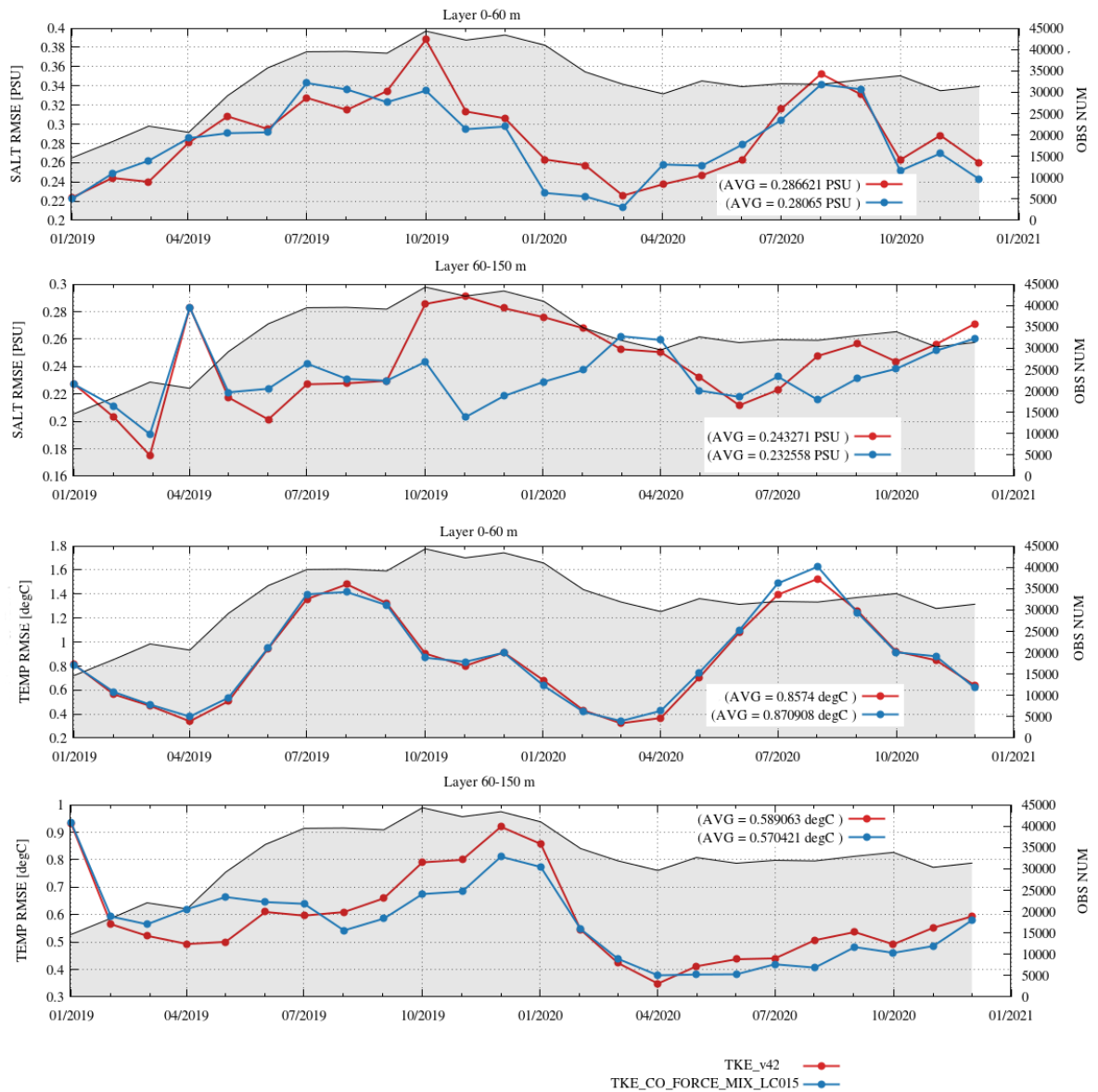


35



CMCC Technical Notes

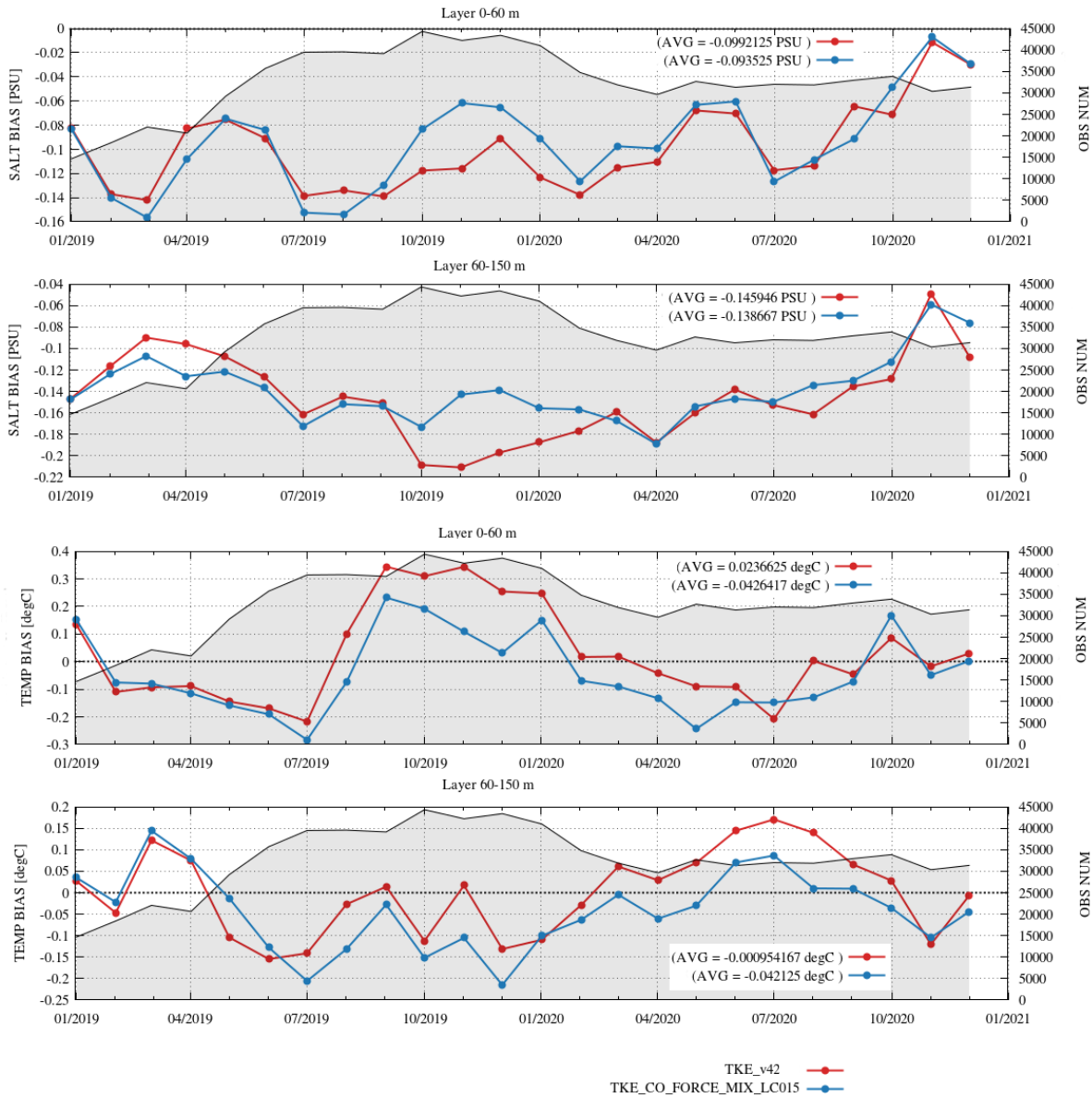
Figure 24. Monthly mean salinity [PSU] (1st and 2nd panels) and temperature [°C] (3rd and 4th panels) RMSD evaluated comparing the daily mean model outputs with respect to in-situ observations for the 2-year period 2019-2020 for the whole Mediterranean Sea and averaged along 2 vertical layers (0-60m and 60-150m). The red and blue lines are showing respectively for the uncoupled experiment (TKE_v42) and the fully coupled experiment (TKE_CO_FORCE_MIX_LC015).





Assessment of wave-current effects on the circulation in the Med-MFC system

Figure 25. Monthly mean salinity [PSU] (1st and 2nd panels) and temperature [°C] (3rd and 4th panels) BIAS evaluated comparing the daily mean model outputs with respect to in-situ observations for the 2-year period 2019-2020 for the whole Mediterranean Sea and averaged along 2 vertical layers (0-60m and 60-150m). The red and blue lines are showing respectively for the uncoupled experiment (TKE_v42) and the fully coupled experiment (TKE_CO_FORCE_MIX_LC015).



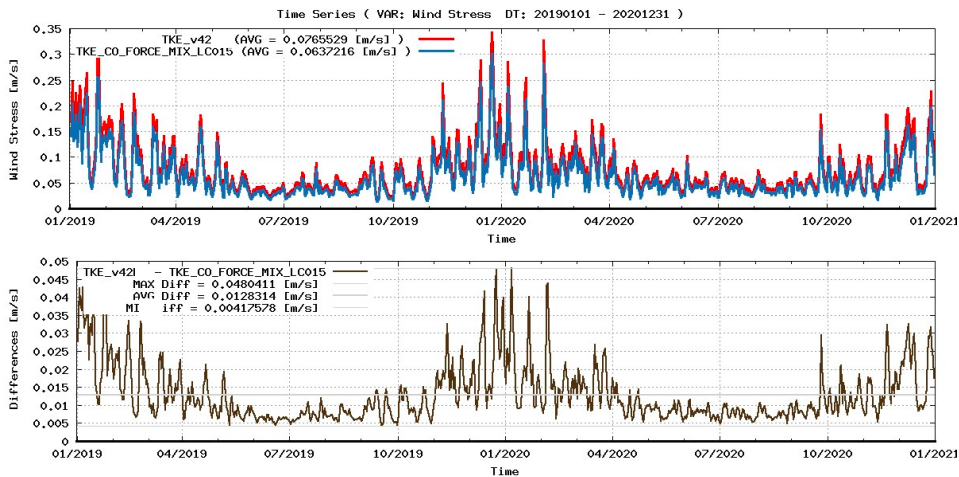


6.2- ASSESSMENT OF THE WAVE-CURRENT INTERACTIONS IN THE MEDSEA

A first assessment of the impact of the wave coupling in the Mediterranean Sea is provided to analyse the surface wind stress.

The wind stress daily time series integrated in the whole Mediterranean domain is presented for the uncoupled TKE_v42 and coupled TKE_CO_FORCE_MIX_LC015 experiments in Figure 26. As in Clementi et al. (2017a), when the neutral drag coefficient from the wave model is used to evaluate the wind stress, the latter is reduced up to 20%. The reduction is larger during winter when stronger winds are blowing. Intensification in the wind stress is localised in time and area of strong wind events that induce wind-waves. The wind stress changes due to the coupling with waves in our simulations are very localised in time and space and it is thus difficult to conclude on their direct effect on upper-ocean dynamics.

Figure 26. Time series of the wind stress [m/s] averaged in the whole Mediterranean Sea (top panel). Wind stress difference between TKE_v42 and TKE_CO_MIX_LC015: mean, minimum and maximum difference values (bottom panel).



The wind stress reduction leads to a decrease of the mixing and reduces the MLD (Figure 27). The histogram of the monthly average distribution of the MLD shows that the experiment coupled only with the surface drag coefficient (TKE_CO_CD) presents



Assessment of wave-current effects on the circulation in the Med-MFC system

shallower MLD in comparison to the uncoupled (TKE_v42) experiment. On the other hand, the wave induced mixing and the Langmuir cells act to increase the mixing and deepen the MLD with respect to the TKE_CO_CD experiment. The full coupled experiment presents a MLD distribution similar to the one of the uncoupled experiment.

Figure 27. Distribution of the monthly mean MLD [m] for the TKE_CO_CD (green), TKE_CO_FORCE_MIX_LC015 (blue) and the uncoupled TKE_v42 (red) experiments.

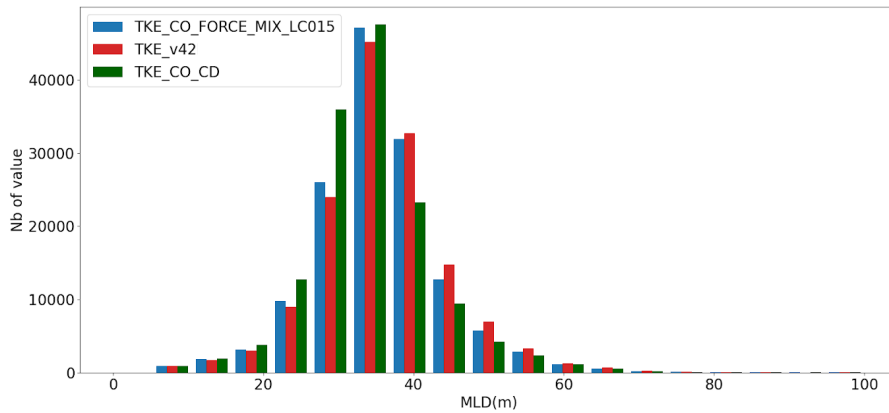
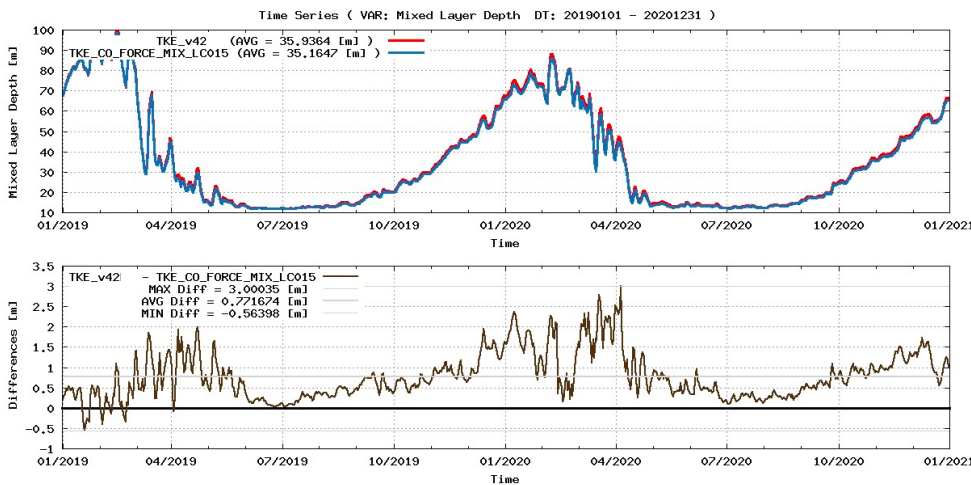


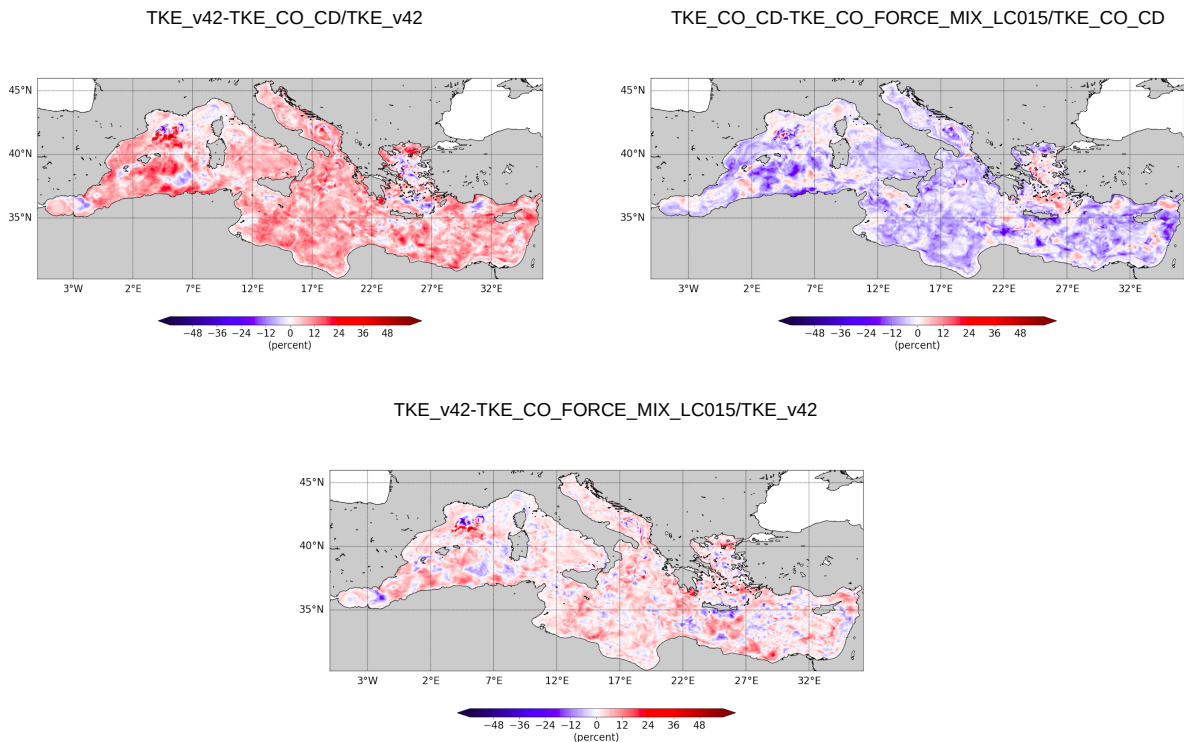
Figure 28. Time series of the MLD [m] averaged in the whole Mediterranean Sea (top panel). MLD differences between TKE_v42 and TKE_CO_MIX_LC015: mean, minimum and maximum difference values (bottom panel).



CMCC Technical Notes

Those processes lead, at basin average, to a slightly deeper mixed layer in winter and a shallower one in the other periods of the year in comparison to the uncoupled simulation (Figure 28). Maps of time mean MLD differences (Figure 29) show that the surface drag from the wave model leads to a decrease of the MLD almost in the whole Mediterranean basin, while the fully coupled experiment increases the MLD with respect to the one including only the surface drag coefficient, but not with respect to the uncoupled experiment. Further investigations based on a short timescale have to be performed to assess the impact of wave coupling during storms.

Figure 29. Maps of MLD time mean (2019) differences [%] between the uncoupled TKE_v42 and TKE_CO_CD (top left), the uncoupled TKE_v42 and TKE_CO_FORCE_MIX_LC015 (top right) and the TKE_CO_CD and TKE_CO_FORCE_MIX_LC015 (bottom).



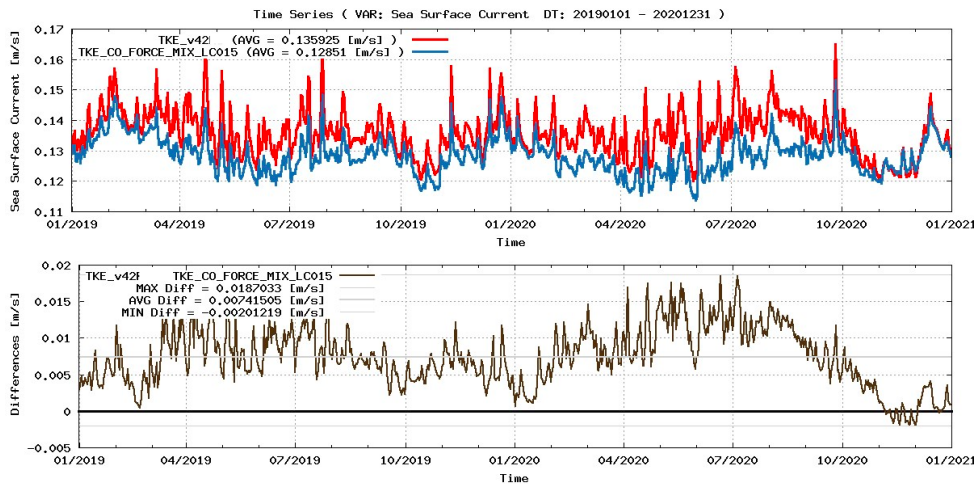
The last analysis evaluates the impact of the surface waves on Mediterranean Sea surface currents and surface kinetic energy (KE). Figure 30 shows a net decrease up



Assessment of wave-current effects on the circulation in the Med-MFC system

to 15% in the magnitude of the quasi-Eulerian sea surface current for the coupled experiment in comparison to the uncoupled sea surface velocity. The basin averaged decrease of sea surface current is higher in spring and summer period than during winter. Differences can be attributed to the lowest basin average wind stress but also to the Stokes–Coriolis force that leads to a decrease in velocities in the whole boundary layer (Rasclé et al., 2008) and to the increased mixing due to waves. Indeed, Couvelard et al. (2020) have shown that the inclusion of vertical mixing due to waves and Langmuir circulation reduces the shear in surface and attenuates the currents in the surface layers. The decrease in surface current magnitude leads to a net decrease in surface KE (up to 20 %) when the coupling with waves is included (Figure 31).

Figure 30. Time series of the uncoupled TKE_v42 Sea Surface Velocity (in red) and of the coupled TKE_CO_FORCE_MIX_LC015 quasi-Eulerian Sea Surface current (blue) [m/s] averaged in the whole Mediterranean Sea (top panel). Sea Surface current differences between TKE_v42 and TKE_CO_MIX_LC015: mean, minimum and maximum difference values (bottom panel).



In the following analysis, the Stokes drift (U_s) is taken into account in order to evaluate the Lagrangian velocity, which is described in the coupled system as the sum between the quasi-Eulerian current and the Stokes drift ($U_L = U_{QE} + U_s$). The basin averaged Stokes drift (Figure 32) has value of about 0.02m/s in the Mediterranean Sea with up to



CMCC Technical Notes

0.08m/s during winter. Differences between the uncoupled velocity from TKE_v4.2 and the Lagrangian velocity from the TKE_CO_FORCE_MIX_LC015 experiments shows a seasonal pattern. The coupled model has the highest velocity (up to 20%) in winter and lower velocity (up to 10%) in summer in comparison with the uncoupled experiment.

Figure 31. Time series of the uncoupled TKE_v42 Surface Kinetic Energy (in red) and of the coupled TKE_CO_FORCE_MIX_LC015 Surface Kinetic (only for the quasi-Eulerian component) (blue) [m²/s²] averaged in the whole Mediterranean Sea (top panel). Surface KE differences between TKE_v42 and TKE_CO_MIX_LC015: mean, minimum and maximum difference values (bottom panel).

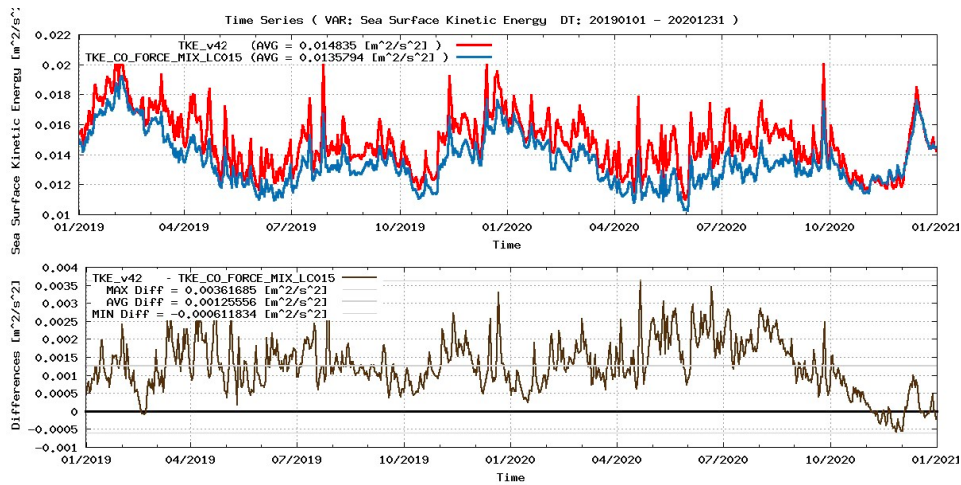
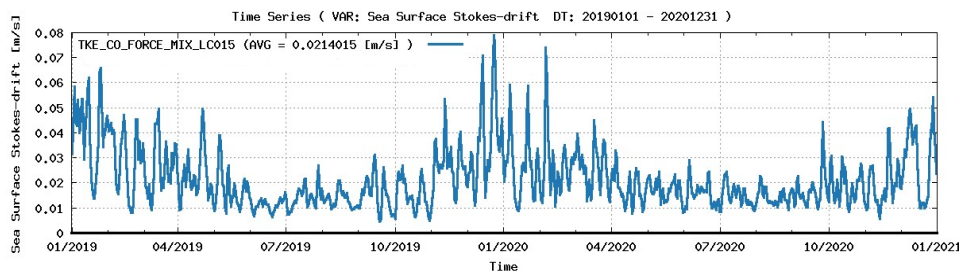


Figure 32. Time series of the surface Stokes-drift [m/s] averaged in the whole Mediterranean Sea.





Assessment of wave-current effects on the circulation in the Med-MFC system

Figure 33. Time series of the uncoupled TKE_v42 Sea Surface current (in red) and of the Lagrangian sea surface current for TKE_CO_FORCE_MIX_LC015 (blue) [m/s] averaged in the whole Mediterranean Sea (top panel). Sea Surface current differences between TKE_v42 and TKE_CO_MIX_LC015: mean, minimum and maximum difference values (bottom panel).

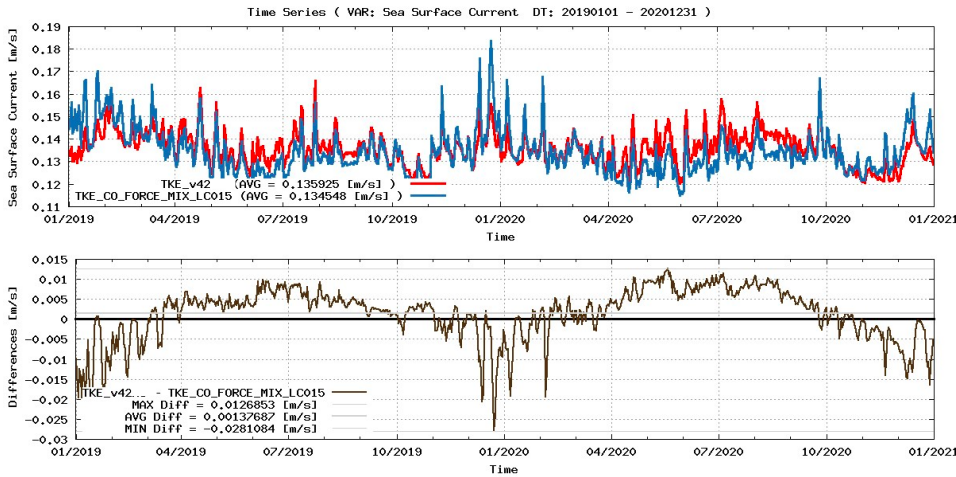
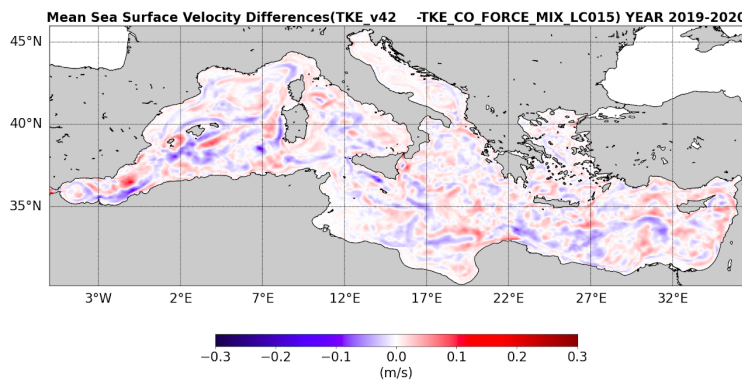


Figure 34: Map of mean Sea Surface velocity time mean (2019-2020) differences [m] between TKE_v4.2 and TKE_CO_FORCE_MIX_LC015.



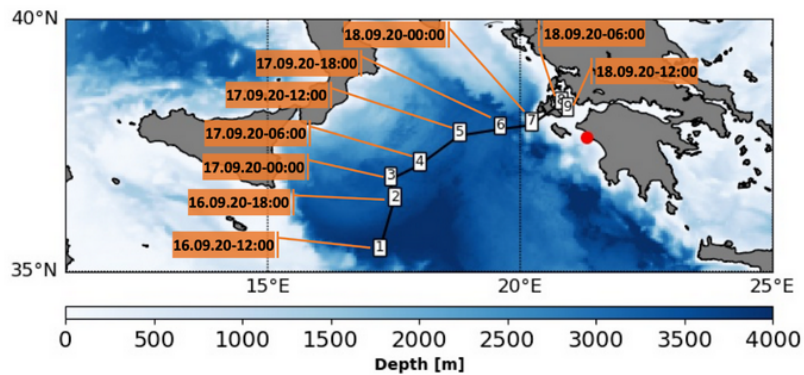
The 2-year period mean velocity difference map shows a stronger impact close to the Gibraltar strait and in the south-western Mediterranean Sea and Levantine Sea whereas region like the Adriatic Sea, Aegean Sea and the western part of the Ionian sea seems to be, in averaged, less affected by the wave coupling.



6.3- IMPACT OF WAVES ON THE IONIAN SEA DYNAMICS DURING MEDICANE IANOS

From 17th to 20th September 2020, Medicane Ianos (cyclone generating in the Mediterranean Sea) hit the Ionian Sea and Greece (Figure 35) with wind speeds up to 110 km/h. The analysis of Medicane Ianos footprint in the Ionian Sea is provided for the uncoupled TKE_v42 and coupled TKE_CO_FORCE_MIX_LC015 experiments.

Figure 35. Model topography, Katakolon Tide Gauge position (red circle), and Ianos path (black line) including dates of the minimum atmospheric pressure locations.



Medicane Ianos evolution in the Ionian Sea is also tracked by means of low pressure centre locations (black line and dates in Figure 35) derived from the ECMWF 6-hours mean sea level pressure analysis fields from 16th to 18th of September. Medicane Ianos moved northward in the first days, followed by an eastward pathway until September 18th when it reached the Greek coastline.

The impact of Medicane Ianos' passage is clearly captured by the uncoupled and coupled hydrodynamic and wave models which simulated an increase of the sea level and significant wave height along the Medicane path as shown in Figure 36. A strong signal occurred on September 17th at 00:00 UTC when the simulated sea level due to the surge reached more than 0.6m and the significant wave height grew to 5.2m. As the system moved eastward, 24 hours later, Medicane Ianos hit the coasts of the

Assessment of wave-current effects on the circulation in the Med-MFC system

Ionian islands, and at that time, the simulated wave heights reached a value of 5m near Zakynthos with sea level of 0.63m.

We can notice that the sea level seems lower in the coupled experiments at the beginning of the Medicane (16th and 17th). After 17th at midday sea level for the uncoupled and coupled simulations are similar close to the Medicane path.

The model hourly mean sea level is compared to observations at the Katakolon Tide Gauge (red point in Figure 35) on the west Peloponnese coast of Greece (Figure 37). The time series of the model results are extracted for the model grid cells closest to the tide gauge. The 25-hourly mean of the sea level measured at the tide gauge is used to remove the tidal signal (detiding) and compare with the model results without tides. The reference levels of the NEMO model and tide gauge observations are different, a constant offset (79cm) is added to the model values, corresponding to the mean difference between the modelled and the observed sea level in the considered period.

As mentioned previously, both uncoupled and coupled simulations show similar results at the end of the Medicane (less than 1cm differences). Results show a general good agreement with the 25-hourly mean of the sea level measured at the tide gauge. Models underestimate the sea level of about 4cm from September 17th until the first hours of September 18th when the peak of the signal is registered. The peak of the signal is well represented by both simulations, with an overestimation of about 1cm.

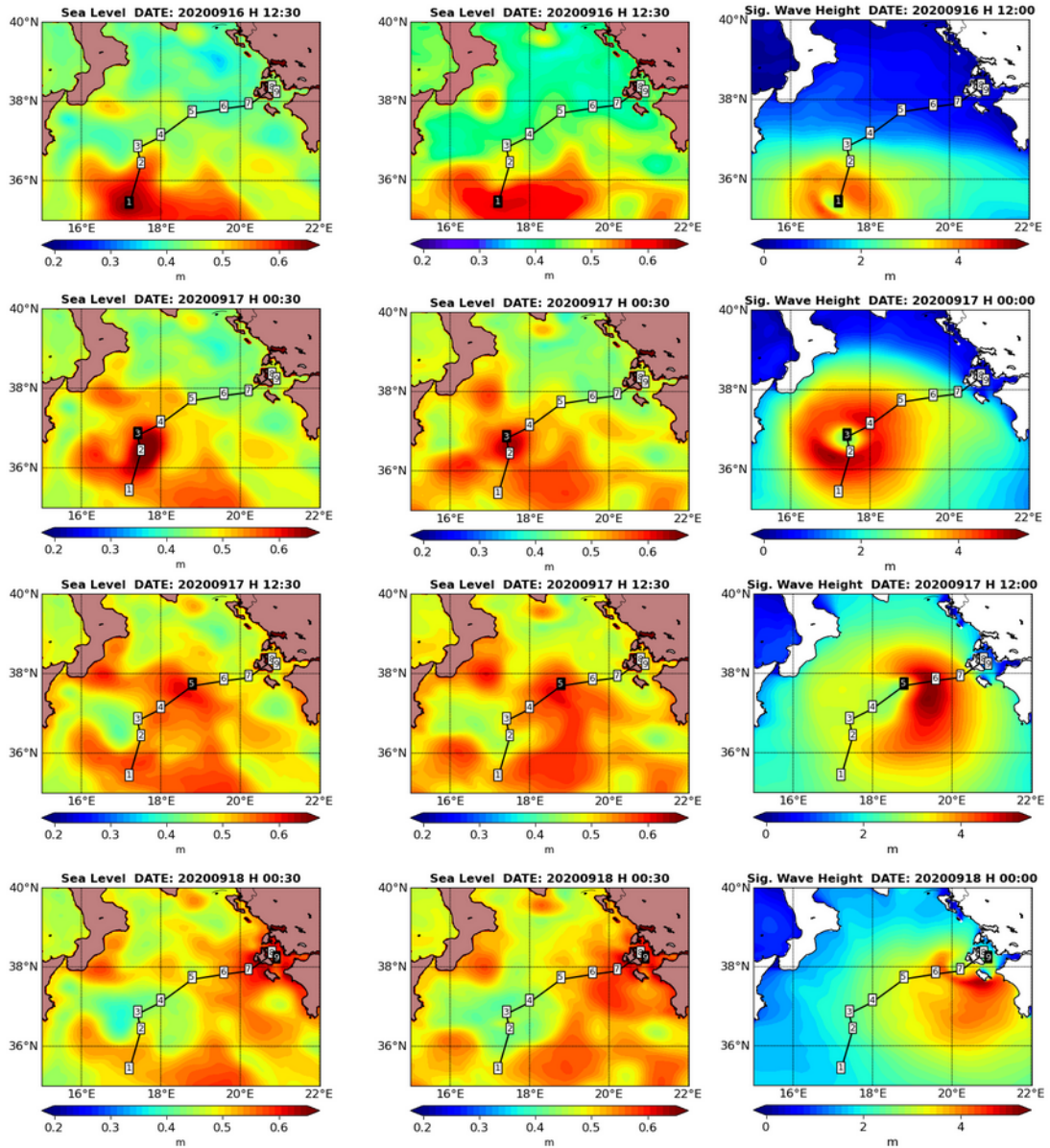


45



CMCC Technical Notes

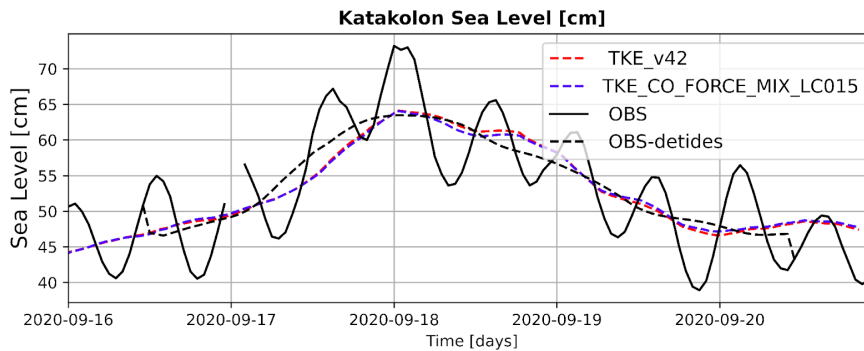
Figure 36. Maps of surface fields from 16th to 18th of September 2020 (every 12 hours): left panels: sea level [m] for the uncoupled experiment; central panels: sea level [m] for the coupled experiments; right panels: significant wave height [m]. The path of the low pressure centres is also provided (black line), from September 16th at 12.00 (n. 1) to September 18th at 12.00 (n. 9) every 6 hours.





Assessment of wave-current effects on the circulation in the Med-MFC system

Figure 37. Time series of sea level measured at Katakolon Tide Gauge (black line) and 25hourly mean (black dashed line), evaluated from the TKE_v42 uncoupled (red dashed line) and from the TKE_CO_FORCE_MIX_LC015 coupled (blue dashed line) experiments.



Numerical results are compared to satellite SST L4 data during the period of interest. Generally, the coupled experiment seems to improve the skills of SST in comparison to satellite data (Figure 38). Indeed, the uncoupled experiment seems to induce not enough reduction of SST in the first days of the Medcane (15th and 16th September) for which no cold structure can be observed in the Ionian Sea. At the time the Medcane impacts the Greek coast (18th September) both uncoupled and coupled runs seem to overestimate the induced cold water by lanos. Two days after the Medcane reached the coast (20th September), the models are underestimating the SST along lanos track, however the coupled experiment seems to have a more persistent cold SST and better reproduce the structure of the satellite data in the southern Ionian Sea.

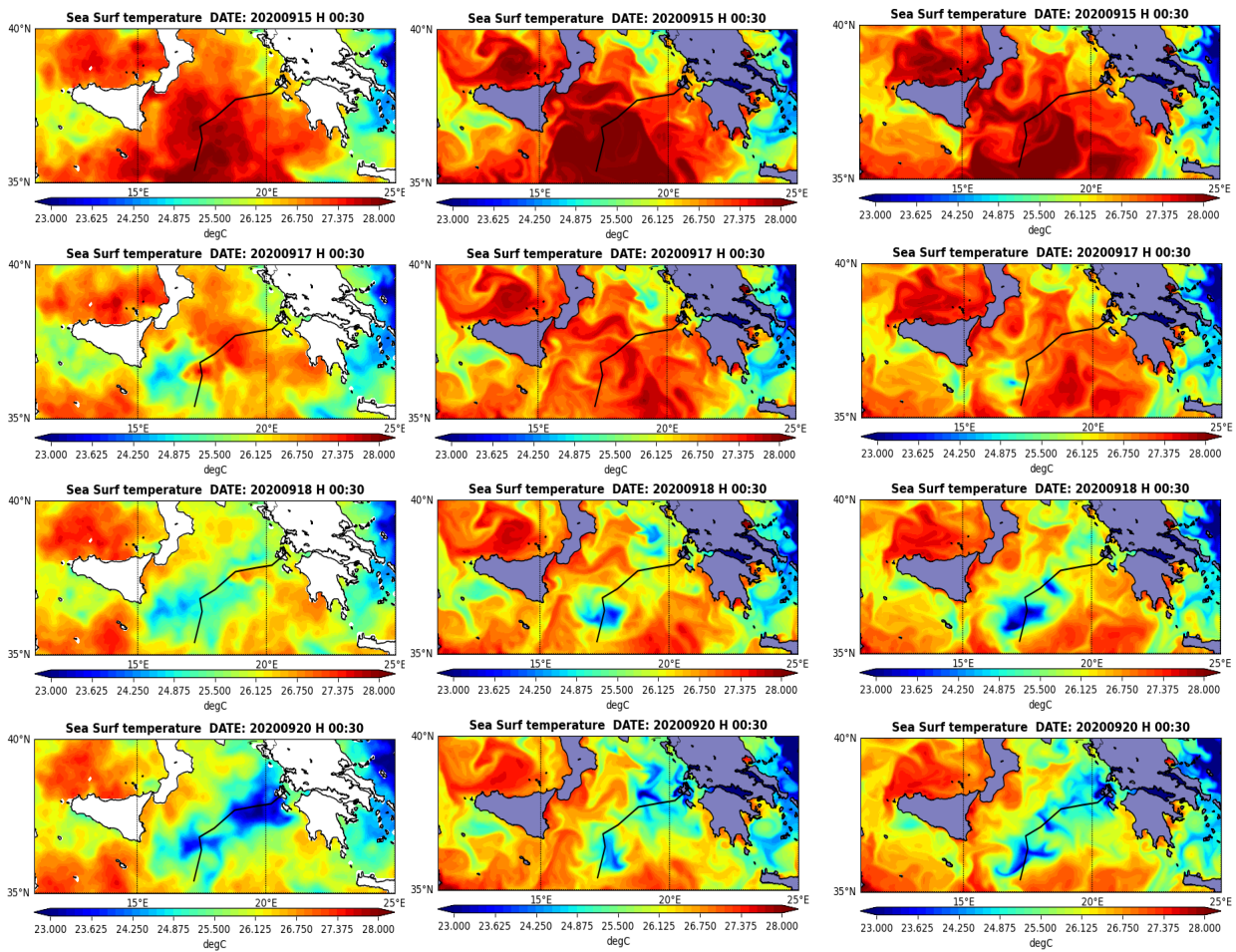
Between 15th and 18th of September, the satellite data show a SST decrease of about 4°C along the Medcane track (Figure 39). Both the uncoupled and coupled experiments are able to describe this decrease in temperature, the coupled simulation presents a decrease in temperature more aligned along the Medcane path and closer to the structure highlighted by the satellite. However, we should consider that this observational dataset could not represent the small scale features present in the model solution due to the scarcity of direct observations along the Medcane track (caused by



CMCC Technical Notes

cloud covering during the event), thus the SST L4 dataset is a combination of a first guess field with available data from previous days.

Figure 38. SST [°C] at different times between September 15th (before Ianos) and September 20th (after Ianos) from satellite data (left), the uncoupled TKE_v42 experiment (middle) and the coupled TKE_CO_FORCE_MIX_LC015 experiment (right) including the Mediane Ianos path from ECMWF surface pressure data (black line).



Ianos also left a footprint in the MLD all along its track (Figure 40). The signal of the Mediane is stronger and more persistent in the coupled experiment in comparison to the uncoupled one.

Assessment of wave-current effects on the circulation in the Med-MFC system

Figure 39. SST [°C] anomaly between September 19th (after lanos) and 15th from satellite data (left), the uncoupled TKE_v42 experiment (middle) and the coupled TKE_CO_FORCE_MIX_LC015 experiment (right) including the Mediane lanos path from ECMWF surface pressure data (black line).

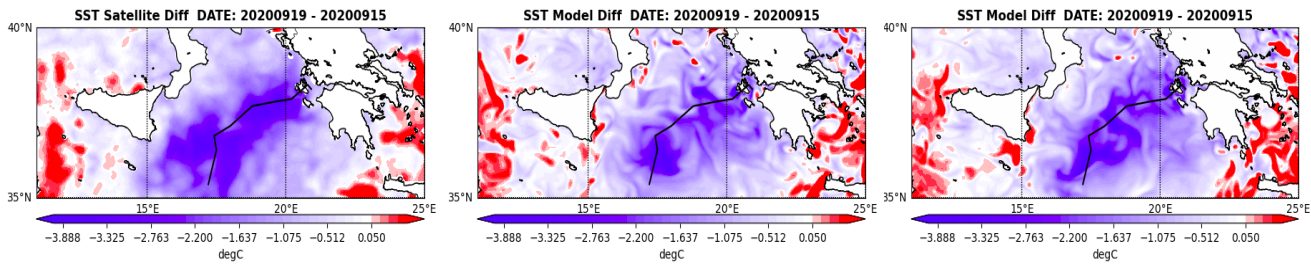
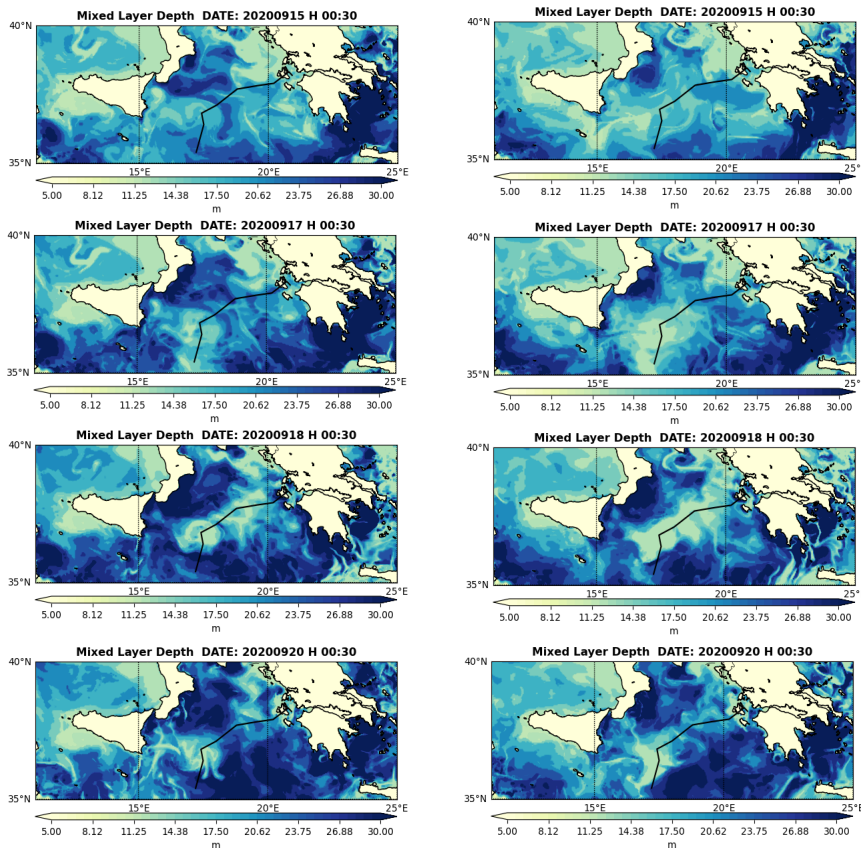


Figure 40. MLD [m] at different times between September 15th (before lanos) and September 20th (after lanos) from the uncoupled TKE_v42 experiment (left) and the coupled TKE_CO_FORCE_MIX_LC015 experiment (right) including the Mediane lanos path from ECMWF surface pressure data (black line).



7- CONCLUSION

This described modeling upgrades implemented in the NEMO v4.2 to improve the wave-current interaction processes and presents the results of a set of experiments carried out in the Mediterranean Sea following as much as possible the modelling implementation of the operational analysis and forecasting system based on NEMO v3.6 developed and implemented at CMCC in the framework of the Copernicus Marine Service.

Thus, as a first step, twin experiments are carried out implementing NEMO v3.6 and NEMO v4.2 in the Mediterranean Sea using the same physical parameterizations and numerical choices. This analysis has highlighted only small differences between the 2 NEMO versions for all the analysed fields which could be caused by the increased numerical precision of the latest NEMO version, but also by the upgraded river runoff module, and the differences between the variable volume (*key_vvl*) option used to run the NEMO v3.6 experiment and the quasi-Eulerian coordinate (*key_qco*) used for the NEMO v4.2 experiment. These changes have led to a general slight increase of the skill of the NEMO v4.2 results when compared to Copernicus Marine *in-situ* and satellite observational datasets.

As a second step, a set of experiments including wave-current interaction processes are carried out for 1 year (including a 1 year spin-up) by coupling 1-way online NEMO v4.2 with the wave model WW3 v6.07 by means of the OASIS coupler. Different levels of complexity are tested including in NEMO: the surface drag coefficient, the Stokes Drift, Stokes-Coriolis, Vortex Force, Bernoulli head, modified TKE accounting for breaking waves, modified Langmuir turbulence. The analysis of the modelling results shows that the surface drag coefficient from the wave model is decreasing the surface wind stress thus reducing the mixed layer depth, while when including the whole set of wave-current interaction processes the mixing is increased and the mixed layer depth is deepened. The modified wind stress as well as the Stokes-Coriolis and the wave-induced mixing are reducing the quasi-Eulerian surface



Assessment of wave-current effects on the circulation in the Med-MFC system

current of about 15%. Moreover, the choice of the adimensional Langmuir parameter has shown to be of great importance for the Mediterranean Sea dynamics, thus a proper calibration would be needed. The model validation has then shown that the fully coupled experiment provides on average the best skill when comparing temperature and salinity with respect to *in-situ* and satellite observational datasets.

The analysis of Ianos Mediane shows a significant change of the surface ocean fields such as an increase of sea level, significant wave height, and a decrease of surface temperature during the event for both the uncoupled and ocean-wave coupled simulations. The ocean wave coupled system reproduces better the reduction of SST compared to the observations available in the area and during the period of interest

ACKNOWLEDGEMENTS

This work has been carried out in the framework of the IMMERSE H2020 Project (Grant agreement ID: 821926, DOI 10.3030/821926) and the Copernicus Marine Service for the Mediterranean Monitoring and Forecasting Service.

BIBLIOGRAPHY

Ardhuin, F., Rogers, E., Babanin, A., Filipot, J., Magne, R., Roland, A., der Westhuysen, A. V., Queffeuilou, P., Lefevre, J., Aouf, L., and Collard, F.: Semiempirical dissipation source functions for ocean waves. part i: Definition, calibration, and validation. *JPO*, 40:1917–1941, 2010.

Ardhuin, F., Jenkins, A., Hauser, D., Reniers, A., and Chapron, B.: Waves and operational oceanography : Toward a coherent description of the upper ocean. *EOS*, 86:37–39, 2005.

Axell, L. B.: Wind-driven internal waves and Langmuir circulations in a numerical ocean model of the southern Baltic Sea, *J. Geophys. Res.*, 107, 25–1–25–20, doi:[10.1029/2001JC000922](https://doi.org/10.1029/2001JC000922), 2002.

Battjes, J., and Janssen, J.: ENERGY LOSS AND SET-UP DUE TO BREAKING OF RANDOM WAVES. *Coastal Engineering Proceedings*, 1(16), 32, doi:[10.9753/icce.v16.32.1978](https://doi.org/10.9753/icce.v16.32.1978).

Belcher, S. E., Grant, A. L. M., Hanley, K. E., Fox-Kemper, B., Van Roekel, L., Sullivan, P. P., Large, W. G., Brown, A., Hines, A., Calvert, D., Rutgersson, A., Pettersson, H., Bidlot, J.-R., Janssen, P. A. E. M., and Polton, J. A. : A global perspective on Langmuir turbulence in the ocean surface boundary layer, *Geophys. Res. Lett.*, 39, L18605, doi:[10.1029/2012GL052932](https://doi.org/10.1029/2012GL052932), 2012.

Breivik, Ø., Mogensen, K., Bidlot, J.-R., Balmaseda, M. A., and Janssen, P.: Surface Wave Effects in the NEMO Ocean Model: Forced and Coupled Experiments, *J. Geophys. Res.-Oceans*, 120, 2973–2992, doi:[10.1002/2014JC010565](https://doi.org/10.1002/2014JC010565), 2015.

Breivik, Ø., Bidlot, J.-R., and Janssen, P. A. E. M.: A Stokes drift approximation based on the Phillips spectrum, *Ocean Model*, 100, 49–56, doi:10.1016/j.ocemod.2016.01.005, 2016.

Cavaleri, L., Fox-Kemper, B., and Hemer, M.: Wind waves in the coupled climate system. *Bull Amer Meteor Soc*, 93:1651–1661, 2012.

Clementi, E., Oddo, P., Drudi, M., Pinardi, N., Korres, G. and Grandi A.: Coupling hydrodynamic and wave models: first step and sensitivity experiments in the Mediterranean Sea. *Ocean Dynamics*, doi:10.1007/s10236-017-1087-7, 2017a.

Clementi, E., Pistoia, J., Delrosso, D., Mattia, G., Fratianni, C., Storto, A., Ciliberti, S., Lemieux, B., Fenu, E., Simoncelli, S., Drudi, M., Grandi, A., Padeletti, D., Di Pietro, P., and Pinardi, N.: A 1/24 degree resolution Mediterranean analysis and forecast modelling system for the Copernicus Marine Environment Monitoring Service. Extended abstract to the 8th EuroGOOS Conference, Bergen, 2017b

Couvelard, X., Lemarié, F., Samson, G., Redelsperger, J.L., Ardhuin, F., Benshila, R., Madec, G.: Development of a 2-way coupled ocean-wave model: assessment on a global NEMO(v3.6)-WW3(v6.02) coupled configuration, *Geosci. Model Dev.*, 13, 3067–3090, doi:10.5194/gmd-13-3067-2020, 2020.

Craig, A., Valcke, S., and Coquelart, L.: Development and performance of a new version of the OASIS coupler, OASIS3-MCT_3.0. *Geoscientific Model Development*, Vol 10, Issue 9, doi:10.5194/gmd-10-3297-2017, 2017.



CMCC Technical Notes

Craik, A. D. D. and Leibovich, S.: A rational model for Langmuir circulations, *J Fluid Mech*, 73, 401–426, doi:10.1017/S0022112076001420, 1976.

Delrosso, D.: Numerical modelling and analysis of riverine influences in the Mediterranean Sea, PhD thesis, 2020.

Estubier, A., and M. Levy, Notes Techn. Pole de Modelisation IPSL, 2000.

Fekete, B. M., Vörösmarty, C. J., and Grabs, W.: Global, Composite Runoff Fields on Observed River Discharge and Simulated Water Balances Rep. 22, 113 Global Runoff Data Cent., Koblenz, Germany, 1999.

Hasselmann, L.: On the mass and momentum transfer between short gravity waves and larger-scale motions, *J- Fluid Mech*, vol 50, pp189-205, 1971

Hasselmann, S., and Hasselmann, K.: Computations and parameterizations of the nonlinear energy transfer in a gravity wave spectrum. Part I: a new method for efficient computations of the exact nonlinear transfer integral. *J Phys Oceanogr*, 15:1369-1377, 1985.

Hasselmann, K.: Ocean circulation and climate change, *Tellus B*, 43, 82–103, doi:10.3402/tellusb.v43i4.15399, 1991.

Hellerman, S., Rosenstein, M.: Normal monthly wind stress over the world ocean with error estimates. *J Phys Oceanogr*, vol 13, 93-104, 1983.

Houpert, L., Testor, P., and Durrieu de Madron, X.: Gridded climatology of the Mixed Layer (Depth and Temperature), the bottom of the Seasonal Thermocline (Depth and

Assessment of wave-current effects on the circulation in the Med-MFC system

Temperature), and the upper-ocean Heat Storage Rate for the Mediterranean Sea. SEANOE. Doi:[10.17882/46532](https://doi.org/10.17882/46532), 2015.

55

Janssen, P. A.: Progress in ocean wave forecasting, *J. Comp. Phys.*, 227, 3572–3594, doi:[10.1016/j.jcp.2007.04.029](https://doi.org/10.1016/j.jcp.2007.04.029), 2008.

Large, W., and Yeager, S.: Diurnal to decadal global forcing for ocean and sea-ice models: the data sets and flux climatologies. CGD NCAR Technical Note: TN-460+STR, pp 111, 2004.

Law Chune, S., and Aouf, L.: Wave effects in global ocean modeling: parametrizations vs. forcing from a wave model, *Ocean Dynam.*, 68, 1739–1758, doi:[10.1007/s10236-018-1220-2](https://doi.org/10.1007/s10236-018-1220-2), 2018.

Leibovich, S.: On wave–current interaction theories of langmuir circulations. *J. Fluid Mechanics*, 99:715–724, 1980.

Madec, G. and the NEMO team: NEMO ocean engine”, NEMO reference manual 3_6_STABLE, Note du Pôle de modélisation, Institut Pierre-Simon Laplace (IPSL), France, No 27 ISSN No 1288–1619, 2016.

Maraldi, C., Chanut, J., Levier, B., Ayoub, N., De Mey, P., Reffray, G., Lyard, F., Cailleau, S., Drévillon, M., Fanjul, E.a., Sotillo, M.G., and Marsaleix, P.: NEMO on the shelf: Assessment of the Iberia-Biscay-Ireland configuration. *Ocean Science* 9, 745–771. doi:[10.5194/os-9-745-2013](https://doi.org/10.5194/os-9-745-2013), 2013.



56

CMCC Technical Notes

Oddo, P., Adani, M., Pinardi, N., Fratianni, C., Tonani, M., and Pettenuzzo, D.: A nested Atlantic-Mediterranean Sea general circulation model for operational forecasting, *Ocean Science*, VOL 5, pp 461–473, doi:10.5194/os-5-461-2009. 2009, 2009.

Oddo, P., Bonaduce, A., Pinardi, N., and Guarnieri, A.: Sensitivity of the Mediterranean sea level to atmospheric pressure and free surface elevation numerical formulation in NEMO. *Geoscientific Model Development*, Vol 7, pp3001–3015, 2014.

Onink, V., Wichmann, D., Delandmeter, P., and Van Sebille, E.: The role of Ekman currents, geostrophy, and Stokes drift in the accumulation of floating microplastic. *Journal of Geophysical Research: Oceans*, 124, 1474–1490, <https://doi.org/10.1029/2018JC014547>, 2019.

Pacanowsky, R.C., and Philander, S.G.H.: Parameterization of vertical mixing in numerical models of tropical oceans. *J. Phys. Oceanogr.*, 11, pp. 1443-1451, 1981.

Pettenuzzo, D., Large, W.G., and Pinardi N.: On the corrections of ERA-40 surface flux products consistent with the Mediterranean heat and water budgets and the connection between basin surface total heat flux and NAO, *J. Geophys. Res.*, 115, C06022, doi:[10.1029/2009JC005631](https://doi.org/10.1029/2009JC005631), 2010.

Polton, J. A., Lewis, D.M., and Belcher, S.E.: The Role of Wave-Induced Coriolis–Stokes Forcing on the Wind-Driven Mixed Layer. *J. Phys. Oceanogr.*, **35**, 444–457, <https://doi.org/10.1175/JPO2701.1>, 2005.

Raich, F.: Note on the flow rates of the Adriatic rivers. Tech. Rep. RF 02/94. CNR, Istituto Talassografico di Trieste, Italy, pp8, 1996.

Raschle, N., and Ardhuin, F.: Drift and mixing under the ocean surface revisited: Stratified conditions and model-data comparisons, *J. Geophys. Res.*, 114, C02016, <https://doi.org/10.1029/2007JC004466>, 2009.

Raschle, N., Ardhuin, F., Queffelec, P., and Croizé-Fillon, D.: A global wave parameter database for geophysical applications. Part 1: wave-current-turbulence interaction parameters for the open ocean based on traditional parameterizations, *Ocean Model.*, 25, 154–171, <https://doi.org/10.1016/j.ocemod.2008.07.006>, 2008.

Shimura, T., Mori, N., Takemi, T., and Mizuta, R.: Long-term impacts of ocean wave-dependent roughness on global climate systems, *J. Geophys. Res. Oceans*, 122, 1995–2011, doi:10.1002/2016JC012621, 2017.

Stokes, G. G.: On the theory of oscillatory waves. *Cambridge Philos Soc.* 8:197–237, 1847.

Tolman, H.: User manual and system documentation of WAVEWATCH III™ version 3.14. NOAA/NWS/NCEP/MMAB Tech. Note 276, pp 194, 2009.

Tolman, H.: Distributed memory concepts in the wave model wavewatch iii. *Parallel Computing*, 28:35–52, 2002.

Tolman, H. L. Alleviating the Garden Sprinkler Effect in wind wave models *Ocean Modelling*, 4(3-4), 269-289, 2002a.

Tolman, H. L.: Validation of WAVEWATCH III version 1.15 for a global domain. Tech. Note 213, Environmental Modeling Center, College Park Maryland, USA, 33 pp, 2002b.



58

CMCC Technical Notes

Tonani, M., Balmaseda, M., Bertino, L., Blockley, E., Brassington, G., Davidson, F., Drillet, Y., Hogan, P., Kuragano, T., Lee, T., Mehra, A., Paranathara, F., Tanajura, C. and Wang, H.: Status and future of global and regional ocean prediction systems, *Journal of Operational Oceanography*, DOI:[10.1080/1755876X.2015.1049892](https://doi.org/10.1080/1755876X.2015.1049892), 2015.

Tonani, M., Pinardi, N., Dobricic, S., Pujol, I., and Fratianni, C.: A high-resolution free-surface model of the Mediterranean Sea, *Ocean Sci.*, 4, 1–14, doi:10.5194/os-4-1-2008, 2008

van den Bremer, T.S., and Breivik, Ø.: Stokes drift. *Phil. Trans. R. Soc. A* 376: 20170104, <http://dx.doi.org/10.1098/rsta.2017.0104>, 2017.

van Leer, B.: Towards the Ultimate Conservative Difference Scheme, V. A Second Order Sequel to Godunov's Method, *J. Com. Phys.*, 32, 101–136, 1979.

WAVEWATCH III Development Group: User manual and system documentation of WAVEWATCH III R© version 6.07. Tech.Note 333, NOAA/NWS/NCEP/MMAB, College Park, MD, USA, 465 pp, 2019.